ACS APPLIED BIO MATERIALS
Cite This: ACS Appl. Bio Mater. 2019, 2, 5349−5365
Forum Article
www.acsabm.org

Supramolecular Assembly of Amino Acid Based Cationic Polymer for Efficient Gene Transfection Efficiency in Triple Negative Breast Cancer

Rima Saha,[†] Sagar Bhayye,[‡] Shuvam Ghosh,[†] Achintya Saha,[‡] and Kishor Sarkar*[,†]

[†]Gene Therapy and Tissue Engineering Lab, Department of Polymer Science and Technology and [‡]Drug Design and Chemoinformatics Lab, Department of Chemical Technology, University of Calcutta, 92, A.P.C. Road, Kolkata - 700009, India

Supporting Information

ABSTRACT: The success of gene therapy is enormously dependent on an efficient gene carrier, and in this context, cationic polymers still continue to play a major role particularly with respect to the safety issue compared to viral vectors. Developing an efficient gene carrier system having promising gene transfection efficiency with low toxicity is the foremost impediment associated with a nonviral carrier. Here, we explored amino acid based biocompatible polymers synthesized via reversible addition−fragmentation chain transfer (RAFT) polymerization where glycine (Gly), leucine (Leu), and phenyl alanine (Phe) amino acids were used as the pendent groups of the polymeric brushes. The presence of both a hydrophobic group (long chain aliphatic group associated with the RAFT agent) and hydrophilic amino groups was associated with the supramolecular assembly of the polymeric chain having hydrodynamic sizes within the range of 150−300 nm with a positive zeta potential of 30 ± 5 mV. All polymers showed very low toxicity and possessed >80% cell viability even at a very high concentration of 1000 μg/mL against both normal and cancerous cells. In addition to this, the polymers also showed excellent blood compatibility, and negligible hemolysis was observed at the concentration of 500 μg/mL. All polymers showed efficient DNA complexation capability as well as excellent protection of DNA against highly negatively charged surfactant and enzymatic digestion, although the efficiency was dependent on the N/P ratio of polymer/DNA complexes. Interestingly, the phenyl alanine moiety containing polymer brush P(HEMA−Phe−NH_2) showed a hexagonal shaped nanoparticle after complexation with pDNA and consequently showed higher cellular uptake, resulting in a higher transfection efficiency in a triple negative breast cancer cell, the MDA-MB-231 cell. Therefore, the synthesized polymer containing an amino acid pendent group, especially the phenyl alanine moiety, may be a promising nonviral gene carrier system in gene therapy application in the future.

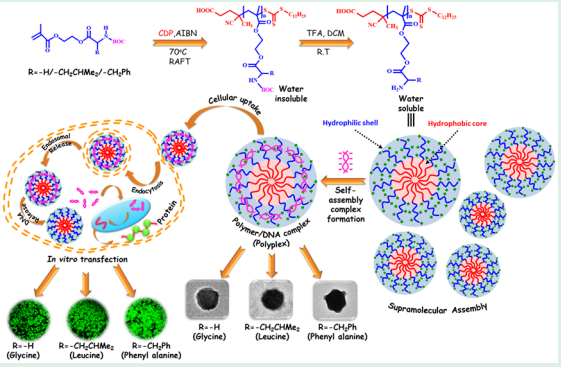

KEYWORDS: *amino acid based cationic polymers, RAFT polymerization, triple negative breast cancer, gene therapy, blood compatibility, low toxicity*

INTRODUCTION

Triple negative breast cancer (TNBC) is considered as the most aggressive type of breast cancer among all other forms of breast cancers, with 15−20% contribution.[1] Due to the lack of the estrogen receptor (ER), progesterone receptor (PR), and human epidermal growth factor receptor 2 (HER-2) expression,[2] the treatment of TNBC becomes challenging. Despite the initial response of chemotherapy for TNBC patients, the highly metastatic nature of the TNBC tumor increases the number of deaths inversely.[3−6] In addition to this, the inherent toxicity of chemotherapeutic drugs limits the long-term treatment of TNBC patients.[7]

Over the past decade, gene therapy has shown a great hope as an alternative promising therapeutic technique for the treatment of genetic diseases such as Alzheimer's, Parkinson's disease,[8] cardiovascular diseases (CVD),[9] and even cancer.[10,11] Despite the development of several gene delivery vectors over the past few years, an efficient and safe gene delivery vector remains challenging for successful gene therapy application.

Recently, nonviral gene delivery vectors such as cationic lipids, liposomes, cationic polymers including polyethylenimine (PEI),[12] fluorinated polyethylenimine (FPEI),[13] and polyamidoamine dendrimer (PAMAM),[14,15] fluorinated cationic polymers,[16−18] graphene,[19] chitosan,[20,21] and so on have gained tremendous attention for gene delivery application because of their ease of synthesis, scope for versatile modification, low toxicity, and nonimmunogenicity over their

Special Issue: Biomaterials Research in India

Received: July 16, 2019
Accepted: October 11, 2019
Published: October 25, 2019

DOI: 10.1021/acsabm.9b00639
ACS Appl. Bio Mater. 2019, 2, 5349−5365

viral counterparts.[22−24] Over the past few years, various nonviral vectors have been developed with improved transfection efficiency in various cells, but efficient gene carrier toward the TNBC cell remains undiscovered. Maincent et al. reported only 4−7% transfection efficiency in MDA-MB-231 cells with Eudragit RS 100 and RL 100 cationic nanoparticles, which was compared to that of commercialized Lipofectamine 2000 (LF2K).[25] In another study, Martinez-Fong's group showed little improved transfection efficiency (∼18%) in MDA-MB-231 cells using a neurotensin−polyplex nanocarrier.[26] Therefore, there is a great demand for an efficient nonviral gene carrier system for TNBC gene therapy. In this concern, amino acid based cationic polymers might be a promising candidate as an alternative nonviral vector because of their biocompatibility, nontoxicity, stimuli responsiveness, and biodegradable nature.[27−29]

Reversible addition−fragmentation chain transfer (RAFT) polymerization is one of the most versatile methods of controlled free radical polymerization, as it allows facile tuning of the molecular architecture of the polymers along with specific molecular weight, molecular weight distributions, and different architectures.[30] Most importantly, it is compatible with a wide range of reaction conditions and does not require any potentially toxic transition metal as used in atom transfer radical polymerization (ATRP).

In order to investigate the effect of the aromatic moiety and aliphatic moiety on the gene complexation capability and ultimately on transfection efficiency, we synthesized three different polymer brushes containing glycine, leucine, and phenyl alanine as the pendent groups. The synthesis of all monomers and polymers was confirmed by FTIR, NMR, and DLS. In vitro cytotoxicity of the polymers was observed on both cancerous and normal cells. The DNA complexation capability of the polymers and the polymer/DNA complexes was also characterized by agarose gel electrophoresis assay and TEM, respectively. Molecular docking analysis was used to study the binding mode and molecular interactions of the polymers with pDNA at different sequences. Further molecular dynamics simulation was also performed on the polymer/DNA complex to observe the stability of the interactions. In vitro transfection efficiency and intracellular uptake kinetics were investigated against MDA-MB-231 triple negative breast cancer cells. The stability of the polymer/DNA complexes was further checked against negatively charged surfactant as well as enzyme to observe its suitability for in vivo application.

EXPERIMENTAL SECTION

Materials. Boc−glycine (Boc−Gly−OH, 99%), Boc−L-leucine (Boc−L-Leu−OH, 99%), Boc−L-phenylalanine (Boc−L-Phe−OH, 99%), trifluoroacetic acid (TFA, 99.5%), heparin sodium salt, and solid iodine were purchased from Sisco Research Laboratories Pvt. Ltd., India. Anhydrous *N*,*N*-dimethylformamide (DMF, 99.9%), 4-dimethylaminopyridine (DMAP, 99%), dicyclohexylcarbodiimide (DCC, 99%), 2-hydroxyethyl methacrylate (HEMA, 97%), 1-dodecanethiol (≥98%), sodium hydride (60% dispersion in mineral oil), branched polyethylenimine (bPEI, 25 kDa), and 4,4-azobis(4-cyanovaleric acid) (≥98%) were obtained from Sigma-Aldrich. Azobis(isobutyronitrile) (AIBN, Sigma, 98%) was recrystallized from methanol prior to the use. Carbon disulfide was purchased from Loba Chemie (99.9%). $CDCl_3$ (99.8% D) and D_2O (99% D) were procured from Cambridge Isotope Laboratories, USA. Some common solvents such as hexanes, acetone, ethyl acetate, dichloromethane (DCM), and so on were purified by standard procedures prior to use.

A DNase I (1 unit/μL) assay kit was purchased from Fermentas, Thermo Scientific, India. Dulbecco's modified Eagle's medium (DMEM), Dulbecco's phosphate-buffered saline (DPBS), dimethyl sulfoxide (DMSO, cell culture grade), molecular grade water, penicillin−streptomycin, trypsin−EDTA solution (0.25% trypsin and 0.02% EDTA in DPBS), and fetal bovine serum (FBS) were bought from Himedia Laboratories Pvt. Ltd., India. 3-(4,5-Dimethylthiazol-2-yl)-2,5-diphenyltetrazolium bromide (MTT), ethidium bromide, and Triton X-100 were obtained from Sisco Research Laboratories Pvt. Ltd., India. 4′,6-Diamidino-2-phenylindole (DAPI) and paraformaldehyde were procured from Sigma. pGL3 control vector (5.25 kb) with an SV-40 promoter was purchased from Promega (Madison, WI, USA). Plasmid DNA (pDNA) encoded with enhanced green fluorescence protein (eGFP-N1) was kindly donated by Dr. Kaushik Chatterjee, IISc, Bangalore, India. pDNA was propagated in a *Escherichia coli* (*E. coli*) DH5-Alpha strain and isolated by a QIAGEN Midiprep kit (USA) according to the manufacturer's protocol. The purity of pDNA was confirmed by spectrophotometry (A_{260}/A_{280}), and the corresponding concentration was determined from its absorbance at 260 nm.

Synthesis of Chain Transfer Agent (CTA). 4-Cyano-4-(dodecylsulphanylthiocarbonyl)sulphanyl pentanoic acid (CDP) was used as a CTA for the RAFT polymerization here. CDP was synthesized according to a previous report with slight modification.[31] In brief, a measured amount of 1-dodecanethiol (5 g, 24.7 mmol) was added to a solution of sodium hydride (0.62 g, 25.8 mmol) in diethyl ether (50 mL) placed in a three-necked jacketed reactor kept in a nitrogen environment at a temperature of 5−10 °C. Immediately, a vigorous evolution of hydrogen was observed, while grayish sodium hydride was transformed to a thick white slurry indicating the formation of sodium thiododecylate. After the reaction mixture was cooled to 0 °C, carbon disulfide (1.9 g, 24.9 mmol) was added dropwise to the above reaction mixture, and a thick yellow precipitate of sodium *S*-dodecyl trithiocarbonate resulted. The yellow product of *S*-dodecyl trithiocarbonate was filtered subsequently and used directly for the next step of the reaction after drying at room temperature under vacuum for overnight.

Solid iodine (2.54 g, 10 mmol) was added portion wise to a stirring solution of sodium *S*-dodecyl trithiocarbonate (5.96 g, 19.8 mmol) in diethyl ether (41 mL). Thereafter, the reaction mixture was allowed to stir at room temperature for 1 h; the formation of white precipitation indicated the formation of sodium iodide as a byproduct, which was subsequently removed by filtration. The yellowish filtrate was washed with an aqueous solution of sodium thiosulfate in order to quench excess iodine and dried over anhydrous sodium sulfate, a residue of bis(dodecylsulfanylthiocarbonyl) disulfide was obtained after evaporation of solvent, and the product was used in the next step without further purification.

Finally, 4,4-azobis(4-cyanovaleric acid) (2.27 g, 8.1 mmol) and bis(dodecylsulfanylthiocarbonyl) (3 g, 5.4 mmol) were taken in ethyl acetate (54 mL) and refluxed for 18 h. After the solvent was removed, the crude product was extracted with water (twice) to obtain 4-cyano-4-(dodecylsulfanylthiocarbonyl) sulfanyl pentanoic acid (CDP), which was further purified by recrystallization from cold hexane. Finally, purified CDP was isolated as a pale yellow solid having a melting point (mp) of 58 °C (Figure S2, Supporting Information) (Yield: 85%). FTIR (Figure S2, Supporting Information, $\tilde{\nu}$, cm^{-1}): 2920 and 2853 (C−H str.), 1726 (C=O str. of −COOH), 2300 (−CN str.). ^{1}H NMR (Figure S3, Supporting Information, $CDCl_3$, δ, ppm): 0.882 (t, 3H, $C\bar{H}_3$), 1.24 (br s, 18H), 1.7 (m, 2H), 1.87 (s, 3H, $C\bar{H}_3$), 2.64−2.7 (m, 4H, $C\bar{H}_2C\bar{H}_2$), 3.31 (t, 2H, $SC\bar{H}_2$).

Synthesis of Amino Acid Based Vinyl Monomers. Amino acid based vinyl monomers were synthesized by esterification of a Boc-protected amino acid and HEMA in the presence of DCC according to a previously reported work with minor changes.[32] In this work, three different Boc-protected amino acids such as Boc−Gly−OH, Boc−L-Leu−OH, and Boc−L-Phe−OH were used, and the reaction details with one amino acid are given here. Briefly, 8.71 g of DCC (42.2 mmol) was dissolved in 35 mL of dry DCM in a 100 mL three necked round-bottom flask. The flask was purged with dry nitrogen

DOI: 10.1021/acsabm.9b00639
ACS Appl. Bio Mater. 2019, 2, 5349−5365

for 20 min followed by the addition of 5 g of HEMA (38.42 mmol) dropwise into it under continuous stirring, keeping the reaction temperature below 4 °C. Subsequently, 6.73 g (38.4 mmol) of Boc−Gly−OH dissolved in 27 mL of DCM was added to the above solution dropwise with constant stirring. The esterification reaction was carried out in the presence of DMAP (0.42 g, 3.4 mmol), and the reaction was continued for 30 min at 4 °C followed by at room temperature for another 24 h. After completion of the reaction, white precipitate of DCU was removed by filtration, and the obtained colorless filtrate was washed with water twice followed by saturated sodium bicarbonate solution and then by brine solution. After the solution was dried over anhydrous sodium sulfate, a pale yellow colored viscous liquid was obtained after rotary evaporation. Finally, the colorless Boc−HEMA−Gly monomer was obtained after purification by column chromatography (230−400 mesh silica gel) using hexane/ethyl acetate (5% ethyl acetate in hexane) as the mobile phase followed by rotary evaporation. Boc−HEMA−Leu and Boc−HEMA−Phe monomers were synthesized following a similar method as described above.

Boc−HEMA−Gly. (Yield: 92%): FTIR (Figure S4, Supporting Information, $\tilde{\nu}$, cm^{-1}): 3360 (N−H str), 2981 and 2930 (C−H str), 1717 (C=O str), 1637 (C=C str), 1517 (N−H def), 1455, 1401, 1292, 1246, 1190, 1147 (C−O), 1064, 953, 865.

^{1}H NMR (Figure S5, Supporting Information, $CDCl_3$, δ, ppm): 1.472 (s, 9H, Boc), 1.96 (s, 3H, $C=CCH_3$), 3.96 (s, 2H, $OCOC\bar{H}_2NHCO$), 4.40 and 4.42 (s, 2H, $COC\bar{H}_2NH$), 4.40−4.42 (m, 4H, $OC\bar{H}_2C\bar{H}_2O$), 5.63 (s, 1H, $N\bar{H}COO$), 5.63 and 6.15 (s, 2H, $C\bar{H}_2{=}C(CH_3)CO$).

^{13}C NMR (Figure S6, Supporting Information, $CDCl_3$, δ, ppm): 19 (b), 28.5 (k), 43 (h), 63 (f), 64 (e), 77.3 ($CDCl_3$), 80.5 (j), 127 (a), 136.5 (c), 156.5(i), 168 (d), 171 (g).

Boc−HEMA−Leu. (Yield: 81%): FTIR (Figure S4, Supporting Information, $\tilde{\nu}$, cm^{-1}): 3375 (N−H str), 2960, and 2933 (C−H str), 1714 (C=O str), 1639 (C=C str), 1505 (N−H def), 1453, 1393, 1369, 1296, 1155 (C−O), 1049, 944.

^{1}H NMR (Figure S5, Supporting Information, $CDCl_3$, δ, ppm): 0.87 (d, 6H, $((C\bar{H}_3)_2CHCH_2)$, 1.38 (s, 9H, Boc), 1.63 (t, 1H, $(CH_3)_2C\bar{H}CH_2$), 1.87 (t, 2H, $(CH_3)_2CHC\bar{H}_2$), 1.97 (s, 3H, $C=CCH_3$), 4.02−4.07 (m, 4H, $OC\bar{H}_2C\bar{H}_2O$), 4.25 (m, 1H, $(C\bar{H}CH_2CH(CH_3)_2)$, 5.53 and 6.05 (s, 2H, $C\bar{H}_2{=}C(CH_3)CO$).

^{13}C NMR (Figure S6, Supporting Information, $CDCl_3$, δ, ppm): 18.5 (b), 23 (n), 25 (m), 28.5 (k), 42 (l), 52 (h), 77.2 ($CDCl_3$), 80.5 (j), 126.5 (a), 136.5 (c), 155 (i), 167 (d), 173(g).

Boc−HEMA−Phe. (Yield: 89%): FTIR (Figure S4, Supporting Information, $\tilde{\nu}$, cm^{-1}): 3367 (N−H str.), 2974, and 2934 (C−H str.), 1716 (C=O str.), 1635 (C=C str.), 1503 (N−H def), 1452, 1369, 1294, 1252, 1167 (C−O), 1056, 950.

^{1}H NMR (Figure S5, Supporting Information, $CDCl_3$, δ, ppm): 1.29 (s, 9H, Boc), 1.83 (s,3H, $C=CCH_3$), 2.94−2.99 (m, 2H, $C\bar{H}_2C6H_5$), 4.19−4.25 (m, 4H, $OC\bar{H}_2C\bar{H}_2O$), 4.51 (s, 1H, $C\bar{H}CH_2C_6H_5$), 4.9 (s, 1H, $N\bar{H}COO$), 5.49 and 6.01 (s, 2H, $C\bar{H}_2{=}C(CH_3)CO$), 7.008−7.186 (m, 5H, C_6H_5).

^{13}C NMR (Figure S6, Supporting Information, $CDCl_3$, δ, ppm): 19 (b), 29 (k), 39 (l), 55 (h), 63 (f), 63.5(e), $CDCl_3$ (77.2), 80.5 (j), 127 (a), 156 (i), 167.5(d), 172 (g).

RAFT Polymerization. The polymerization was carried out following a procedure depicted by Kumar et al.[33] with some minor changes. In brief, CDP (0.028 g, 0.069 mmol) was dissolved in anhydrous DMF (3.5 mL) in a 50 mL two necked round-bottom flask. After the CDP solution was purged with dry nitrogen for 20−25 min, AIBN (2 mg, 0.014 mmol) dissolved in dry DMF was added by a 5 mL syringe. After that, Boc−HEMA−Gly (1 g, 3.48 mmol) was added to the reaction mixture at 70 °C with constant stirring under a nitrogen atmosphere for a predetermined time. Polymerization was quenched by cooling the mixture in an ice water bath and exposing it to the atmosphere. The thick yellow solid was diluted with acetone and precipitated into cold hexane. The polymer P(Boc−HEMA−Gly) was reprecipitated five times in a similar technique and finally dried under vacuum at 40 °C for 5 h to obtain a pale yellow solid (conversion 73.2%). The synthesis of the polymer was confirmed by ^{1}H NMR and FTIR spectroscopy. The number-average molecular weight (M_n) and polydispersity index (PDI) were determined by gel permeation chromatography (GPC). A similar polymerization procedure was adopted for the polymerization of Boc−HEMA−Leu and Boc−HEMA−Phe monomers to obtain the polymers of P(Boc−HEMA−Leu) (conversion 59.6%) and P(Boc−HEMA−Phe) (conversion 68.4%), respectively.

Deprotection of Boc Moiety. In order to obtain free amine ($-NH_2$) terminated polymer, the Boc moiety was removed from the Boc-protected polymers according to the following procedure. Typically, 0.8 g of P(Boc−HEMA−Gly) was dissolved in 16 mL of DCM followed by dropwise addition of TFA (8 mL) in an ice cold condition. After that, the reaction was allowed to continue for 2 h at room temperature with constant stirring. The completion of deprotection was monitored by precipitating the reaction mixture in cold diethyl ether. After complete deprotection, the precipitate was collected through centrifugation of the reaction mixture at 7000 rpm for 20 min followed by drying under vacuum at 40 °C for 10 h to obtain a pale yellow solid of P(HEMA−Gly−NH_2). Similar process was used to get the Boc-deprotected polymers of P(HEMA−Leu−NH_2) and P(HEMA−Phe−NH_2). The Boc deprotection was confirmed by ^{1}H NMR and FTIR spectroscopy.

Characterization of the Polymers. ^{1}H NMR spectra were carried out on a Bruker DPX 500 MHz NMR spectrometer using $CDCl_3$ and D_2O as solvent. Chemical shifts were reported in ppm using tetramethylsilane (TMS) as an internal standard. Fourier transform infrared (FTIR) analysis was carried out with a PerkinElmer Spectrum 100 FTIR spectrometer equipped with an attenuated total reflection (ATR) module. The sample was uniformly mixed with potassium bromide (KBr) at a 1:10 weight ratio, and KBr pellets were prepared using 10 ton of hydraulic pressure for 10 min at room temperature. After that, FTIR spectra of the pellets were recorded within the frequency range of 4000−500 cm^{-1} for eight consecutive scans at 1 cm^{-1} resolution.

The molecular weight (M_n) and molecular weight distribution or polydispersity index (PDI) were determined by GPC using THF as a mobile phase at 35 °C with a flow rate of 0.9 mL min^{-1}. The system consisted of one Polar Gel-M guard column (50 × 7.5 mm), two Polar Gel-M analytical columns (300 × 7.5 mm), a Waters HPLC pump (Model 515), and a Waters refractive index (RI) detector (Model 2414). Poly(methyl methacrylate) (PMMA) was used as a standard sample to produce the calibration curve.

The particle size of three different polymers were determined by dynamic light scattering (DLS). DLS measurement was carried out by an argon ion laser system tuned at 514 nm using a Zetasizer Nano ZS (Malvern Panalytical, UK). Prior to measurement, all samples were filtered through a 0.2 μm (Millipore) syringe filter directly into a cleaned DLS cuvette with a 10 mm path length. Then, the zeta potential of all polymers was measured with the same instrument at 37 °C. Each measurement was repeated three times to obtain the average value, and the data was represented as a mean of three consecutive measurements (±SD).

Preparation of Polymer/DNA Complexes. Polymer/DNA complexes (polyplexes) were prepared by a complex coacervation method according to the previous study.[34−37] In brief, all polymers and pDNA were dissolved in molecular biology grade solvent separately. Thereafter, equal volumes of polymer solution and pDNA solution were mixed at different N/P ratios (nitrogen to phosphate ratio) of 1:1, 5:1, 10:1, 15:1, 20:1, 40:1, 60:1, 80:1, 100:1, 150:1, and 200:1 in such a way that each N/P ratio contains 0.5 μg of pDNA. Immediately, the polymer/pDNA solution mixtures were vortexed for 15−30 s with a cyclomixer (Vortexer, Heathrow Scientific) and incubated at room temperature for 30 min to allow the formation of polyplexes.

Agarose Gel Electrophoresis Assay. The formation of polyplexes was confirmed by an agarose gel electrophoresis assay. Agarose gel (0.8%, w/w) was prepared in TAE buffer (40 mmol/L of Tris acetate, 1 mmol/L of EDTA) containing ethidium bromide (10 μg/mL) as a pDNA visualizer. Freshly prepared polyplexes as described above were loaded in the respective lanes after mixing with

DOI: 10.1021/acsabm.9b00639
ACS Appl. Bio Mater. 2019, 2, 5349−5365

loading dye (6× gel loading dye, Himedia). The gel was then run at 100 V for 40 min using a Consort power supply (Model: EV2650, Cleaver Scientific, UK). The picture of the gel was captured by a BIOTOP gel doc system (Fluorshot EVO SC750, China).

Characterization of the Polyplexes. The morphology and size of the polyplexes were determined by transmittance electron microscopy (TEM). Freshly prepared polyplexes at an N/P ratio of 100 were deposited on a 300 mesh carbon coated copper grid. After the grid was dried at room temperature overnight, the images were taken by high resolution transmission electron microscopy (HRTEM) (JEM 1010, JEOL, Japan) operated at 200 kV.

The particle size as well as surface zeta potential of the polyplexes at different N/P ratios of 0, 5:1, 10:1, 20:1, 40:1, 60:1, 80:1, and 100:1 were measured at different pHs (pH = 5.5, 7.4, and 8.0). Freshly prepared polyplexes at different N/P ratios containing 1.0 μg of pDNA in each N/P ratio were diluted to 1 mL of DNase-free molecular grade water and then filtered through a 0.2 μm syringe filter prior to the measurement. DLS measurement was performed using an argon ion laser system tuned at 514 nm using a Zetasizer Nano ZS (Malvern Panalytical, UK). Then, the zeta potentials of all of the polymers were measured with the same instrument at 37 °C. Each measurement was carried out in triplicate.

Stability of the Polyplexes in Serum. The stability of the polyplexes in DMEM media was investigated by measuring the particle size of the polyplexes by dynamic light scattering. Polyplexes, namely P(HEMA−Gly−NH_2)/pDNA, P(HEMA−Leu−NH_2)/pDNA, and P(HEMA−Phe−NH_2)/pDNA, at an N/P ratio of 100:1 were prepared and incubated for 30 min at 37 °C in order to ensure complete polyplex formation. Each sample was then diluted with 900 μL of supplemented DMEM (10% FBS) or serum-free DMEM to determine the serum or salt stability of the polyplexes. Prior to measurement, all the samples were filtered through a 0.2 μm syringe filter, and particle size was measured by an argon ion laser system tuned at 514 nm using a Zetasizer Nano ZS (Malvern Panalytical, UK) at certain time intervals of 0, 30, and 90 min. Each measurement was repeated thrice to obtain the average value of particle size, and the data have been represented as a mean of three consecutive measurements (±SD).

Resistance of Polyplexes against Heparin. P(HEMA−Gly−NH_2)/pDNA, P(HEMA−Leu−NH_2)/pDNA, and P(HEMA−Phe−NH_2)/pDNA complexes at an N/P ratio of 100:1 were prepared. After 30 min of incubation, 6 μL of heparin solution at different concentrations ranging from 0.01 to 2 mg/mL were added to the polyplexes and further incubated for 30 min at 37 °C. After that, all the complexes were loaded into the predetermined lane of 0.8% (w/v) agarose in a tris−acetate−EDTA (TAE) buffer, electrophoresis was performed at 100 V for 40 min, and corresponding images were captured by a BIOTOP gel doc system.[38]

DNase I Enzymatic Assay. A DNase I enzymatic assay was carried out by using DNase I as a model enzyme according to our previous study.[37] In detail, DNase I (1 unit/1 μg of pDNA) dissolved in PBS containing 5 mM $MgCl_2$ was added to the freshly prepared polyplexes with different N/P ratios such as 10:1, 20:1, 40:1, 60:1, and 100:1. After incubation at 37 °C for 10 min, 0.5 M EDTA solution was added to the above solution mixture and subsequently heated at 65 °C for 10 min to inactivate the DNase I activity. After that, the polyplexes and the digested naked pDNA were loaded in 0.8% agarose gel electrophoresis, and the corresponding image was captured by a BIOTOP gel doc system after running the gel at 100 V for 40 min.

Blood Compatibility Assay. Human blood was collected from a healthy female adult (25 years old) in the presence of EDTA acting as an anticoagulant agent. The whole blood was centrifuged at 2000 rpm at 4 °C for 10 min, and the supernatant plasma was discarded. After the red blood cells were washed with PBS through resuspension and centrifugation two times, 100 μL of diluted red blood cell solution was added to polymer solution at different concentrations of 10, 50, 100, 200, 500, and 1000 μg/mL, and the total volume was adjusted to 1 mL using sterile PBS solution (pH = 7.4). Triton X-100 (1% v/v) and PBS solution were used as positive and negative controls, respectively. After incubation at 37 °C for 90 min, the above solutions were centrifuged at 2000 rpm for 15 min, and the corresponding absorbance of the supernatant was recorded at 578 nm using an ELISA microplate reader (Erba Lisa Scan EM, TRANSASIA, India). The percentage (%) hemolysis was calculated according to the following equation

$$\%\ \text{hemolysis} = \frac{A_s - A_n}{A_p - A_n} \times 100$$

where A_s, A_n, and A_p represent the absorbance of the sample, negative control, and positive control, respectively. All data are presented as a mean of three consecutive measurements (±SD).

Molecular Docking. The DNA sequence of the cloning vector pGL3-Control (U47296.2) in FASTA format was taken from the National Center for Biotechnology Information (NCBI) database.[39] The UCSF Chimera[40] tool was used to build the 3D structure of DNA. Structures of P(HEMA−Gly−NH_2) (n = 35), P(HEMA−Leu−NH_2) (n = 28), and P(HEMA−Phe−NH_2) (n = 29) were drawn using MarvinSketch.[41] All the structures were then energy minimized using UCSF Chimera[40] to correct the geometry.

The structures were prepared for molecular docking by computing Gasteiger[42] charges and merging nonpolar hydrogens using AutoDock tools.[43] Because of a limitation of computational resources, only the DNA sequence of the promotor region (base pair 48 to 250) was considered for molecular docking. A grid for molecular docking was prepared at the center of the DNA with a size of 90 × 130 × 80. Finally, molecular docking was performed using the AutoDock Vina[44] tool. Polymer−DNA docking was repeated based on a binding sequence obtained by using different segments of DNA to verify the docking hypothesis.

Molecular Dynamics. Based on the binding free energy and interaction, the polymer−DNA complex was selected from molecular docking for molecular dynamic (MD) simulation. Simulations of all complexes were performed in Desmond package.[45] All the systems for MD simulation were prepared by using a Desmond system builder. A water box of orthorhombic shape was used to prepare each system. The distance between the polymer−DNA complex and water box was kept at 10 Å to avoid overlapping of periodic images.[46] The TIP3P water model was used to solvate the water box followed by neutralization of systems by an appropriate number of counterions. Optimized potential for liquid simulations (OPLS) force field[47] parameters were assigned to each system. A periodic boundary condition was applied to each system to avoid a boundary effect. The particle mesh Ewald (PME)[48] method was selected to measure the electrostatic interaction with a 10^{-8} tolerance. The bond length between the hydrogen-heavy atom and the internal geometry of the water molecules was constrained by using the SHAKE algorithm.[49] All the systems were then equilibrated in five different steps. In the first step, a simulation ran for 1000 ps in an NVT ensemble with Brownian dynamics at 10 K with small time steps, and solute non-hydrogen atoms were restrained. In the second step, the simulation ran for 120 ps in an NVT ensemble using a Berendsen thermostat[50] keeping the same conditions as in first step. In the third step, the simulation ran in an NPT ensemble using a Berendsen thermostat and a Berendsen barostat; here, a pressure of 1 atm was applied while other conditions were kept constant as in previous steps. In the fourth step, the system was simulated for 120 ps in an NPT ensemble with a temperature of 300 K with other condition constants. The final step of equilibration was simulated in an NPT ensemble for 240 ps with no restraints. After equilibration and relaxation of all the systems was reached, the final production of MD was performed for 100 ns by maintaining a 300 K temperature with the time step of 2 fs in the NPT ensemble. The Nosé−Hoover Thermostat[51] method was used to maintain the temperature during the simulation with a relaxation time of 1 ps. The energy of each system was recorded every 1.2 ps, and the trajectory was captured at every 4.8 ps of time interval.

Circular Dichroism (CD). Circular dichroism (CD) spectra of pDNA, polymers, and the polymer/pDNA complexes were obtained on a JASCO spectropolarimeter (model J-815; JASCO International

DOI: 10.1021/acsabm.9b00639
ACS Appl. Bio Mater. 2019, 2, 5349−5365

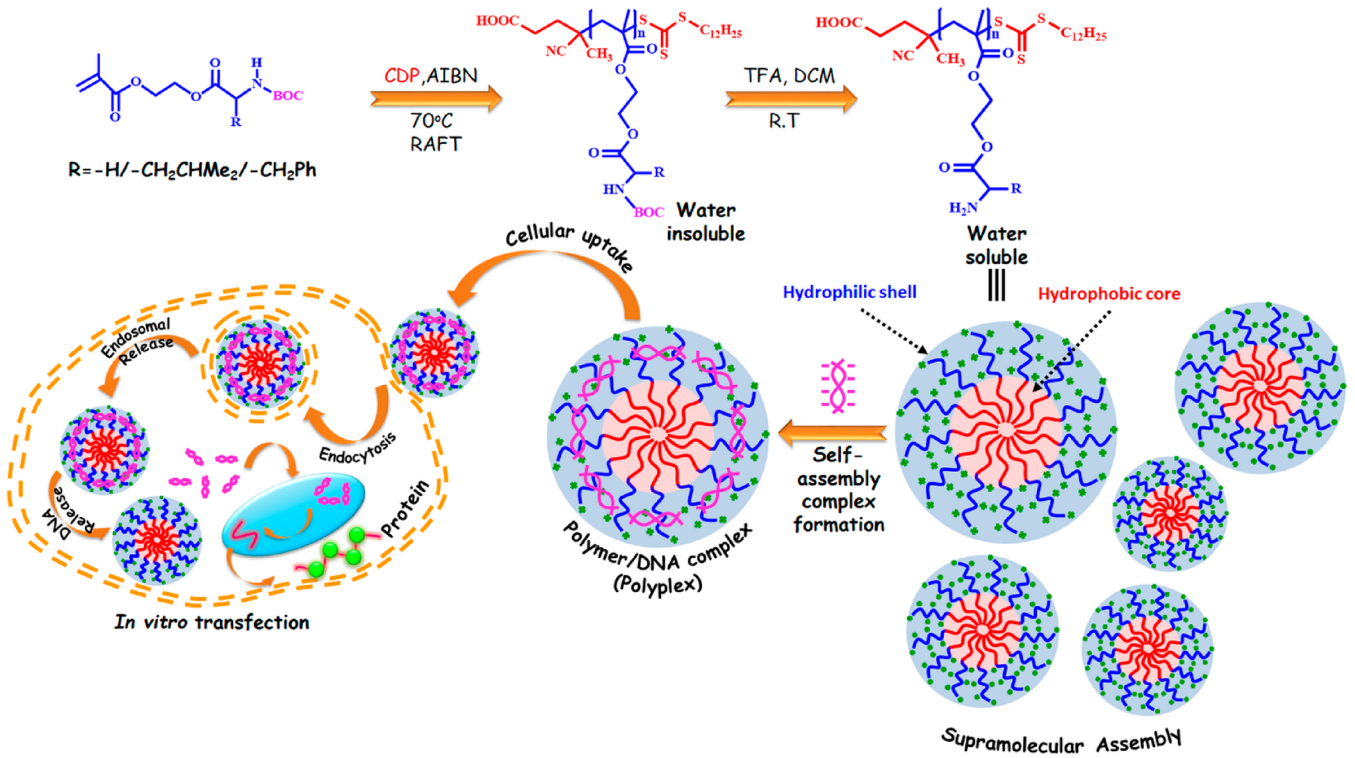

Figure 1. Schematic representation for the synthesis of amino acid based cationic polymers by RAFT polymerization for gene transfection.

Co., Ltd., Tokyo, Japan), using a 1 cm path length cuvette in double distilled water at 25 °C. Prior to the CD spectra measurement, the polyplexes such as P(HEMA−Gly−NH_2)/pDNA, P(HEMA−Leu−NH_2)/pDNA, and P(HEMA−Phe−NH_2)/pDNA complexes were prepared at an N/P ratio of 100:1 and were diluted with water before CD spectra were recorded. Each N/P ratio contained 10 μg of pDNA for complexation. While CD spectra were recorded, the ellipticity values are given in millidegrees (mdeg). The settings for the measurement were 2.0 nm bandwidth, 5 mdeg sensitivity, and three accumulations. Spectra were recorded from 400 to 200 nm at a scan rate of 100 nm/min.

Cell Culture. Triple negative breast cancer cells, MDA-MB-231 cells, were purchased from the National Centre for Cell Sciences (NCCS), Pune, India. The cells were cultured in DMEM supplemented with 10% fetal bovine serum (FBS), 1% antibiotics (penicillin, 100 μg/mL and streptomycin, 100 μg/mL), and 1% of 2 mM L-glutamine at 37 °C in a CO_2 incubator (CelCulture, ESCO, Singapore) maintained at 5% CO_2 and 95% humidity. Cells were subcultured or seeded after reaching 80−90% confluency using 0.25% (w/v) trypsin/0.53 mM EDTA solution.

In Vitro Cytotoxicity Assay. Cells were seeded into a 96-well culture plate at a density of 5 × 10^3 cells per well. After 24 h of incubation, 100 μL aliquots of polymer solutions at different concentrations such as 10, 20, 50, 100, 200, 500, and 1000 μg/mL were added to the cells. PEI, 25 kDa, and untreated cells were used as the positive and negative control, respectively. After 24 h of post-treatment, 100 μL of MTT solution (5 mg/mL) was added to each well after removing the treated solution followed by washing with PBS and incubating at 37 °C for 4 h. Afterward, MTT solution in each well was replaced with 100 μL of DMSO and further incubated for 30 min at 37 °C to dissolve the purple colored formazan crystals. The absorbance was then recorded at 570 nm by an ELISA microplate reader. The experiment was carried out in triplicate. The cell viability (%) was calculated according to the following equation

$$\text{cell viability (\%)} = \frac{OD_{570\,(\text{Sample})}}{OD_{570\,(\text{Control})}} \times 100$$

where $OD_{570\,(\text{Sample})}$ and $OD_{570\,(\text{Control})}$ are the absorbance of the sample and control, respectively, at 570 nm.

In Vitro Transfection. For in vitro transfection, the cells were seeded at a density of 1 × 10^5 cells per well in a 24-well plate containing a sterile coverslip and incubated at 37 °C in a CO_2 incubator maintained at 5% CO_2 and 95% humidity. After reaching 75−80% confluency, the complete media was discarded, and the polyplexes at different N/P ratios of 40:1, 80:1, and 100:1 containing 1 μg of DNA in each weight ratio diluted in serum-free media were added to each well after being washed with DPBS twice. After incubation at 37 °C for 4 h, the transfection solution was removed and washed with DPBS twice followed by the addition of complete media and incubation for another 20 h. Only pDNA and Lipofectamine 2000 (LF2K) were used as the negative and positive control, respectively. After 24 h of post-transfection, the cells were fixed with 4% paraformaldehyde solution after the complete media was removed and then washed with PBS twice. The transfection efficiency was confirmed by observing the green fluorescence protein obtained by eGFP-N1 pDNA using a confocal laser scanning microscope (CLSM, Olympus FV3000) after the coverslip was mounted on a glass slide in the presence of glycerol as mounting media. The transfection efficiency was further quantified by fluorescence-activated cell sorting (FACS) analysis (Beckton-Dickson) using 1 × 10^4 cells per analysis.

Intracellular Kinetics. For intracellular kinetic study, 1 × 10^5 cells suspended in 500 μL of complete DMEM media were seeded on sterile glass coverslips placed in each well of a 24-well plate and cultured for overnight. FITC conjugated polymer/pDNA complexes at an N/P ratio of 100:1 diluted in serum-free media were added to the each well after the culture media was removed followed by washing with DPBS twice. At the predetermined time points such as 0, 0.5, 2, and 4 h, the treated solution was discarded, and the cells were fixed by 4% paraformaldehyde solution after being washed with DBPS twice. The cells were permealized with 1% Triton X-100 solution, and the nuclei were stained with DAPI. The corresponding images were captured by CLSM after the coverslip was mounted on a glass slide using glycerol as mounting media.

DOI: 10.1021/acsabm.9b00639
ACS Appl. Bio Mater. 2019, 2, 5349−5365

Statistical Analysis. All the experiments were carried out in triplicate for reproducibility, and the data are presented as the average value ± standard deviation (SD). Two-way ANOVA was used for statistical analysis, and *, **, ***, and **** were used for *p*-values of <0.05, <0.01, <0.001, and <0.0001, respectively.

RESULT AND DISCUSSION

Polymer Synthesis and Characterization. Amino acid based vinyl monomers were synthesized by esterification of HEMA and Boc-protected amino acids through a carbodiimide coupling reagent. Here, three amino acids such as glycine, leucine, and phenyl alanine were used. The synthesis of monomers was confirmed by FTIR spectroscopy as shown in Figure S1, Supporting Information. Figure S1, Supporting Information shows typical peaks at around 3360, 2980, 1720, 1635, and 1145 cm^{-1}, which correspond to the N−H bond (2° amine), the C−H bond of $-CH_2$, the C=O bond of the ester group, the C=C bond of the vinyl group, and the C−N and C−O bonds, respectively. This result suggests the synthesis of amino acid based vinyl monomers such as Boc−HEMA−Gly, Boc−HEMA−Leu, and Boc−HEMA−Phe. The synthesis of monomers was further confirmed by ^1H and ^{13}C NMR spectroscopy, and the corresponding NMR spectra are shown in Figures S2 and S3, Supporting Information. The corresponding proton and carbon peaks of the respective monomers are summarized above in the Experimental Section. The typical proton peaks for vinyl protons are found at 5.5 and 6.0 ppm, whereas the proton peak for the Boc group is obtained at ∼3.5 ppm. These peaks are also well correlated to the previous reports.[33,52] Therefore, the above data confirm the successful synthesis of amino based vinyl monomers. Here, CDP was used as a RAFT reagent because of the presence of the hydrophobic dodecyl group, which would help for the formation of a supramolecular assembly. The synthesis of CDP was confirmed by DSC, FTIR, and NMR, and the corresponding results are shown in Figures S4−S6, Supporting Information, respectively. The results support well the previous study,[53] which confirms successful synthesis of CDP. The schematic representation of polymer synthesis by RAFT polymerization using CDP as a RAFT reagent and amino acid based vinyl monomers is shown in Figure 1. The synthesis consisted of two consecutive steps including the RAFT polymerization of Boc-protected amino acid based vinyl monomers (Boc−HEMA−Gly, Boc−HEMA−Leu, or Boc−HEMA−Phe) to prepare Boc-protected polymers (P(Boc−HEMA−Gly), P(Boc−HEMA−Leu), or P(Boc−HEMA−Phe)) followed by deprotection of the Boc group using TFA to get amine terminated cationic polymers (P(HEMA−Gly−NH_2), P(HEMA−Leu−NH_2), or P(HEMA−Phe−NH_2)). The synthesis of the Boc-protected polymers was confirmed by FTIR and NMR spectroscopy, and the corresponding spectra are shown in Figures S7 and S8, Supporting Information, respectively. Figure S7, Supporting Information shows a sharp absorption peak at ∼3125 cm^{-1}, which corresponds to N−H stretching of a secondary amine present in a Boc-protected polymer. But after deprotection of the Boc groups, the absorption peak became broad, which may be due to the absorption of moisture by the free primary amine group as shown in Figure 2a. In addition to this, a new peak appeared at 1676 cm^{-1}, which is attributed to the N−H bending of the primary amine group (highlighted by light red color). The FTIR data of both polymers was well supported by NMR data as shown in Figure S8, Supporting Information and Figure 2b−d. In Figure S8, Supporting Information, the presence of the typical peak for protons present in the Boc group at 1.4 ppm indicates the synthesis of Boc-protected polymers, i.e., P(Boc−HEMA−Gly), P(Boc−HEMA−Leu), or P(Boc−HEMA−Phe). However, the peak completely disappeared after deprotection of the Boc-protected polymers by TFA as shown in Figure 2b−d. Apart from this, the presence of the peaks for the protons c, d, and e (assigned for the protons as shown in the chemical structure of polymers (Figure S8, Supporting Information and Figure 2b−d)) in both polymers confirms the synthesis of a polymer containing a pendent amino acid moiety with a free amine group.

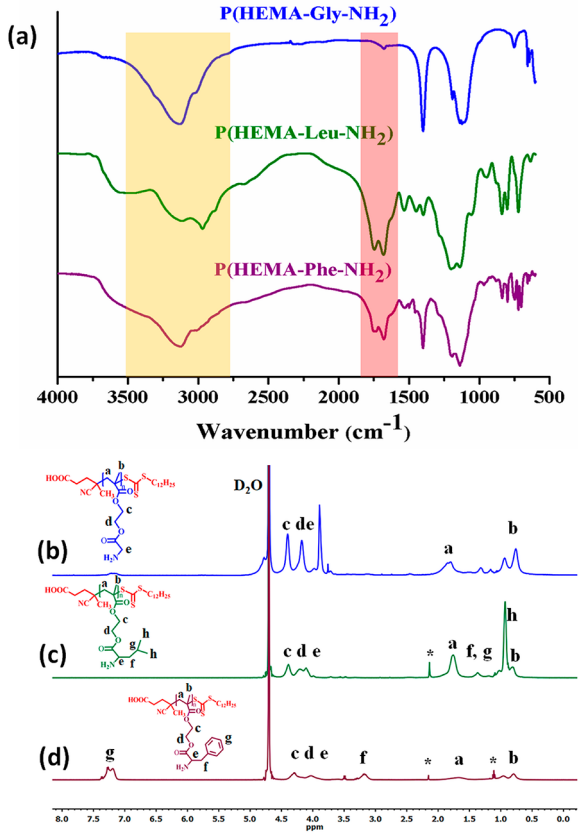

Figure 2. FTIR spectra of P(HEMA−Gly−NH_2), P(HEMA−Leu−NH_2), and P(HEMA−Phe−NH_2) (a) and ^1H NMR spectra of P(Boc−HEMA−Gly) (b), P(Boc−HEMA−leu) (c), and P(Boc−HEMA−Phe) (d).

The molecular weight of the polymers, i.e., P(HEMA−Gly−NH_2), P(HEMA−Leu−NH_2), and P(HEMA−Phe−NH_2), was determined by GPC, and the corresponding values are shown in Table 1. For all polymers, the ratio of [M]:[CTA]:[AIBN] ([monomer]:[chain transfer agent]:[initiator]) was kept constant, i.e., 50:1:0.2, and the obtained molecular weights (number-average molecular weight, M_n) of P(HEMA−Gly−NH_2), P(HEMA−Leu− NH_2), and P(HEMA−Phe−NH_2) were 10.5, 10.0, and 11.3 g mol^{-1}, respectively, which agree well with the molecular weights predicted from theoretical calculation as shown in Table 1. The low polydispersity index (PDI) of all polymers indicates the narrow molecular weight distribution, i.e., equal chain length , which is the main advantage of RAFT polymerization over conventional free radical polymerization. Because of the presence of a hydrophobic dodecyl group and a hydrophilic pendent primary amine group containing an amino acid

DOI: 10.1021/acsabm.9b00639
ACS Appl. Bio Mater. 2019, 2, 5349−5365

Table 1. Details of Different Polymers Including Reactants Feed Ratio, Extent of Conversion, Molecular Weight of Polymers, Hydrodynamic Micelle Size, and Surface Zeta Potential

polymers	[M]:[CTA]:[AIBN]	conv.[a] (%)	$M_{n,Theo.}$[b] (g mol^{-1})	$M_{n,GPC}$[c] (g mol^{-1})	PDI[c]	micelle size[d] (nm)	zeta potential[d] (mV)
P(HEMA−Gly−NH_2)	50:1:0.2	73	10 923	10 548	1.15	158 ± 20	31 ± 3
P(HEMA−Leu−NH_2)	50:1:0.2	60	10 637	10 017	1.15	230 ± 34	25 ± 5
P(HEMA−Phe−NH_2)	50:1:0.2	68	13 312	11 343	1.29	253 ± 60	27 ± 4

[a]Calculated by ^{1}H NMR spectroscopy. [b]Theoretical molecular weight ($M_{n,theo}$) = ($[M]_0/[CTA]_0$ × molecular weight (MW) of [M]) × conversion + (MW of CTA). [c]Measured by GPC using poly(methyl methacrylate) (PPMA) standards in DMF. [d]Measured by DLS using Zetasizer NanoZS.

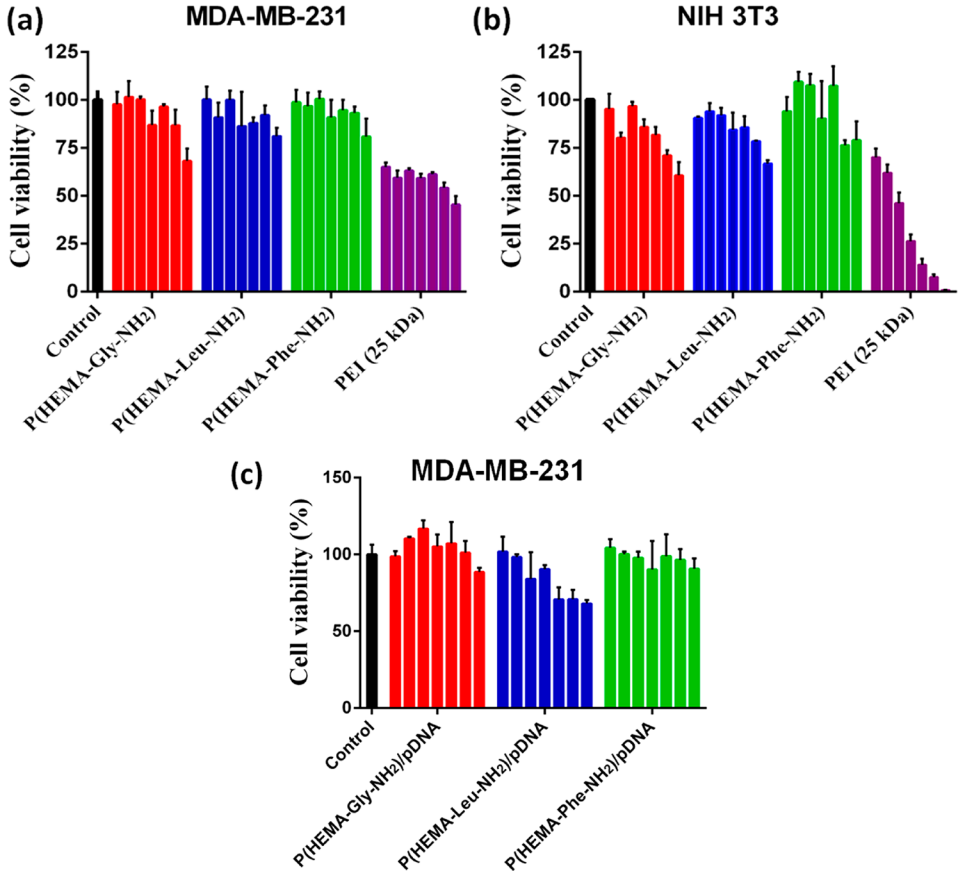

Figure 3. In vitro cytotoxicity of P(HEMA−Gly−NH_2), P(HEMA−Leu−NH_2), P(HEMA−Phe−NH_2), and PEI (25 kDa) at different concentrations of 10, 20, 50, 100, 200, 500, and 1000 μg/mL on MDA-MB-231 (a) and NIH 3T3 (b) cells. Untreated cells were used as a negative control. In vitro cytotoxicity of P(HEMA−Gly−NH_2)/pDNA, P(HEMA−Leu−NH_2)/pDNA, and P(HEMA−Phe−NH_2)/pDNA complexes at the N/P ratios of 10:1, 20:10, 40:1, 60:1, 80:1, 100:1, and 200:1. pDNA (0.5 μg) was used in each N/P ratio (c).

moiety, it is expected that the polymer will form a supramolecular self-assembly micelle in aqueous solution as shown in Figure 1. The hydrodynamic diameter of the micelle was measured by DLS as shown in Table 1, and it is observed that all polymers formed a nanosized micelle having a size within 100−300 nm. Among all the polymers, P(HEMA−Gly−NH_2) showed a smaller micelle with a size of 158 ± 20 nm, but the size slightly increased to 234 ± 34 and then to 253 ± 60 nm with the proton of the glycine moiety substituted by an isopropyl group and the protn of the phenyl group in leucine subsituted by a phenyl alanine moiety, respectively. Because of the presence of free primary amine group in the pendent amino acid moiety of the polymer brush architecture, all polymers showed a positive zeta potential within the range of 25−35 mV as shown in Table 1. Therefore, the polymers may be effective as a nanocarrier of a gene or pDNA through complexation with a gene or pDNA by electrostatic interaction between the positively charged polymer and negatively charged DNA.

In Vitro Cytotoxicity of Polymers. The assessment of cytotoxicity is an important parameter for any material prior to use in the biomedical field. The in vitro cytotoxicity of the polymers was measured by an MTT assay on triple negative breast cancer cells, MDA-MB-231, and fibroblast cells, NIH 3T3,and the corresponding results are shown in Figure 3a,b, respectively. It is observed from Figure 3a that all the polymers showed almost negligible toxicity even at a very high concentration of 1000 μg/mL. However, the glycine based polymer, i.e., P(HEMA−Gly−NH_2), showed a slightly higher toxicity at that concentration compared to the other two polymers, although the cell viability was around 70%, which may be due to a higher zeta potential (31 ± 3 mV, Table 1) of P(HEMA−Gly−NH_2) compared to those of P(HEMA−Leu−NH_2) (25 ± 5 mV) and P(HEMA−Phe−NH_2) (27 ± 4 mV). As cancer cells are more stable compared to normal cells, a cell

DOI: 10.1021/acsabm.9b00639
ACS Appl. Bio Mater. 2019, 2, 5349−5365

viability study using any material on cancer cells may not give assurance of a similar toxicity on normal cells. Therefore, we further carried out the cytotoxicity assay on fibroblast cells, NIH 3T3 cells, as shown in Figure 3b. A similar result was also observed on normal cells as found on cancer cells at all polymer concentrations from 10 to 1000 μg/mL. However, the cell viability slightly decreased at higher concentrations such as 500 and 1000 μg/mL, which may be associated with a higher zeta potential, as a higher zeta potential destabilizes the cellular membrane and consequently results in poor cell viability.[35,36,54] PEI (25 kDa) is considered as the "*gold standard*" for a nonviral gene carrier because of its higher buffering capacity and high transfection efficiency,[12,55] so it was used as the positive control. Even at a very low concentration of 10 μg/mL, PEI showed significant cytotoxicity against the TNBC cel, but the cell viability did not decrease significantly with an increase in the concentration, which may be due to the aggressiveness of the TNBC cell. But the cell viability significantly decreased against normal cells, i.e., NIH 3T3 cells, with an increase in the PEI concentrations, which suggests the severe toxicity of PEI (25 kDa). Therefore, the synthesized polymers can be used safely because of the negligible toxicity to both the cancerous as well as normal cells, where all the polymers showed >70% cell viability even at a very high concentration, i.e., 1000 μg/mL.

Blood Compatibility. Before any biomaterial is used in vivo, it is necessary to check its blood compatibility, as the material will come into contact with blood, and the material should be blood compatible for clinical application. To confirm the blood compatibility of the synthesized polymers, a hemolysis assay was carried out according to the previous studies[20,37] using the polymers at different concentrations of 10, 50, 100, 200, 500, and 1000 μg/mL. PBS and water or Triton X-100 were used as the positive and negative control, respectively. The blood compatibility of the polymers was also compared with that of PEI at the same concentrations, and the corresponding data are shown in Figure 4.

Figure 4a–d shows the digital photograph of the hemolysis of red blood cells (RBCs) in the presence of P(HEMA–Gly–NH_2), P(HEMA–Leu–NH_2), P(HEMA–Phe–NH_2), and PEI (25 kDa) at the concentration range from 10 to 1000 μg/mL. It is observed that the hemolysis of RBC was started by P(HEMA–Leu–NH_2) at the concentration of 500 μg/mL (Figure 4b), whereas the polymer P(HEMA–Phe–NH_2) showed hemolysis at the concentration of 1000 μg/mL (Figure 4c). In comparison, P(HEMA–Gly–NH_2) did not show any hemolysis at any concentration within the concentration range of 10–1000 μg/mL (Figure 4a). Because of the presence of an aliphatic isobutyl group in the leucine-moiety-containing polymer (P(HEMA–Leu–NH_2)), the interaction of this polymer was more with the outer membranes of RBCs through a hydrophobic–hydrophobic interaction, as RBCs mainly contain hydrophobic phosphatidylcholine and sphingomyelin in the outer membrane, which results in more hemolysis compared to the other two polymers.[56] The presence of a phenyl group in P(HEMA–Phe–NH_2) also showed little interaction with the RBC membrane and consequently caused hemolysis at a higher concentration of 1000 μg/mL. In contrast, P(HEMA–Gly–NH_2) does not possess any such hydrophobic groups, and as a result, it did not show any hemolytic effect at any concentration. The blood compatibility of PEI (25 kDa) was also compared with these polymers, as PEI (25 kDa) is considered as a "gold standard"

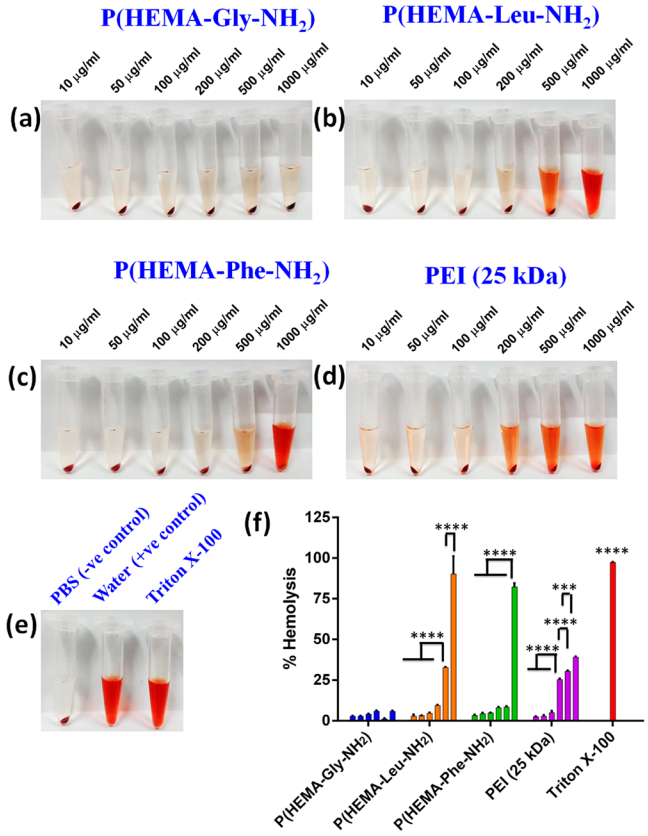

Figure 4. Digital photograph of blood compatibility assay by P(HEMA–Gly–NH_2) (a), P(HEMA–Leu–NH_2) (b), P(HEMA–Phe–NH_2) (c), and PEI (25 kDa) (d) at different concentrations of 10, 50, 100, 200, 500, and 1000 μg/mL and 1× PBS (used as negative control), water, and Triton-X-100 (used as positive control) (e). The represented bar graph of % hemolysis by P(HEMA–Gly–NH_2), P(HEMA–Leu–NH_2), P(HEMA–Phe–NH_2), and PEI (25 kDa) at different concentrations of 10, 50, 100, 200, 500, and 1000 μg/mL (f).

of nonviral gene carriers.[12] From Figure 4d, it is found that PEI (25 kDa) started to show a hemolytic effect at a concentration of 200 ug/mL, which is a much lower contraction than the hemolytic concentration of RAFT polymers. The higher positive zeta potential of PEI may destabilize the cellular membrane of RBC through electrostatic interaction and consequently cause hemolysis of RBC at a comparatively low concentration. The bar graph as shown in Figure 4f shows the quantitative hemolysis of RBC by the different polymers. From Figure 4f, it is observed that the polymers P(HEMA–Leu–NH_2) and P(HEMA–Phe–NH_2) are safe in vivo with a negligible hemolytic effect up to the concentration of 200 μg/mL, whereas P(HEMA–Gly–NH_2) can be used safely comparatively at a higher concentration of 1000 μg/mL.

Agarose Gel Electrophoresis Assay. The basic concept of a cationic polymer as nonviral vector is to form a complex with negatively charged DNA through electrostatic interaction.[20,35–37,54,55] The complexation capability of P(HEMA–Gly–NH_2), P(HEMA–Leu–NH_2), and P(HEMA–Phe–NH_2) with pDNA was evaluated using an agarose gel retardation assay according to previous reports,[34,37,55] and the corresponding gel images are shown in Figure 5. From Figure 5, it is observed that the electrophoretic mobility of pDNA was completely retarded by all the polymers, as the polymers possess a positive zeta potential as shown in Table 1,

DOI: 10.1021/acsabm.9b00639
ACS Appl. Bio Mater. 2019, 2, 5349–5365

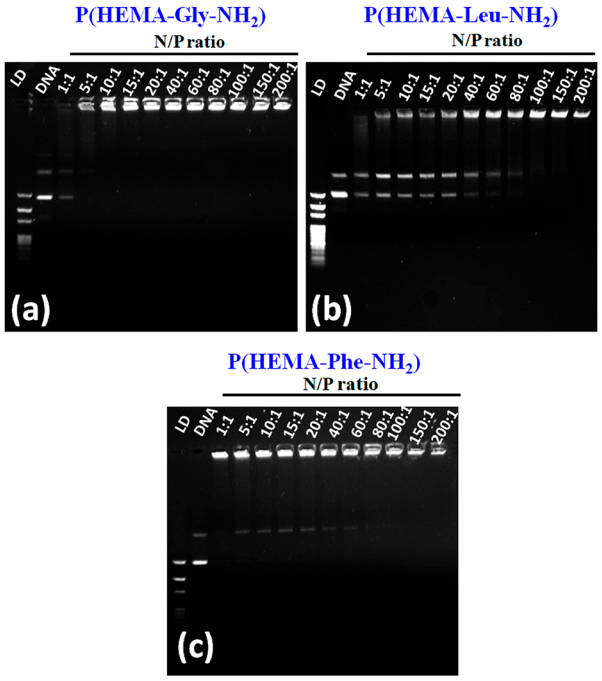

Figure 5. Agarose gel electrophoresis assay of P(HEMA−Gly−NH_2) (a), P(HEMA−Leu−NH_2) (b), and P(HEMA−Phe−NH_2) (c) at different N/P ratios of 1:1, 5:1, 10:1, 15:1, 20:1, 40:1, 60:1, 80:1, 100:1, 150:1, and 200:1.pDNA (0.5 μg) was used in each N/P ratio.

although the retardation of DNA movement was dependent on the N/P ratio. Among all the polymers, P(HEMA−Gly−NH_2) showed a better complexation capability with pDNA and showed complete pDNA complexation at an N/P ratio of 10, where the electrophoretic mobility of pDNA was completely retarded as shown in Figure 5a. In comparison, the movement of pDNA was completely inhibited comparatively at higher N/P ratios of 80 and 40 by P(HEMA−Leu−NH_2) (Figure 5b) and P(HEMA−Phe−NH_2) (Figure 5c), respectively. This fact may be attributed to the respective surface zeta potentials of the polymers. As shown in Table 1, P(HEMA−Gly−NH_2) exhibits a higher positive zeta potential (~31 mV) followed by P(HEMA−Phe−NH_2) (~27 mV) and P(HEMA−Leu−NH_2) (~25 mV). The higher positive zeta potential of P(HEMA−Gly−NH_2) might help to bind more efficiently the negatively charged pDNA at a low N/P ratio of 10. A similar phenomenon was also observed in the previous study, where the magnitude of the positive zeta potential affected the pDNA complexation capability of the carrier.[34] As the difference in the positive zeta potentials of the polymers was not significantly different, the pDNA complexation by the polymers should not vary so much. The molecular architecture of the polymers may have an effect on the complexation with pDNA. Therefore, we further carried out molecular docking and corresponding molecular dynamics to understand the molecular interaction of polymer with the pDNA.

Molecular Docking. In the first attempt, a DNA sequence of 48−250 was used for docking of all polymers. The binding DNA sequences with a binding free energy of each polymer for this region are listed in Table 2. P(HEMA−Phe−NH_2) has shown the highest binding affinity with a binding energy of −2.9 kcal/mol followed by P(HEMA−Leu−NH_2) and P-(HEMA−Gly−NH_2). A lower binding free energy of the polymer−DNA complex suggests a greater affinity of the polymer. Molecular docking analysis shows P(HEMA−Phe−NH_2) has affinity toward the DNA base pair adenosine and thymine. In the case of P(HEMA−Gly−NH_2) and P(HEMA−Leu−NH_2), the binding DNA sequence is found to be mixed with all bases. Based on the binding sequence obtained from this molecular docking experiment, the polymer binding DNA sequences "TTTTTT" for P(HEMA−Phe−NH_2) and "GCTGACTAATT" for the other two polymers are found to be repeated multiple times in DNA after the whole sequence is scanned. Using this information, the DNA sequence of 3282−3323 (n = 41) was selected for P(HEMA−Phe−NH_2), while for the other two sequences, a length of 3261−3304 (n = 43) was selected to verify polymer binding to the same sequence.

In the second molecular docking experiment, it has been observed that the binding sequences of P(HEMA−Gly−NH_2) and P(HEMA−Leu−NH_2) very much remain the same with a marginal increase in binding free energy. In the case of P(HEMA−Phe−NH_2), the binding free energy increased significantly from −2.9 to −3.5 kcal/mol with a change in the DNA binding sequence with the addition of cytosine and guanine base pairs. Polymer−DNA complexes with a binding free energy obtained from molecular docking are depicted in Figure 6. Polymers established contact with DNA through hydrogen bonding, π−cation, and salt bridge interactions.

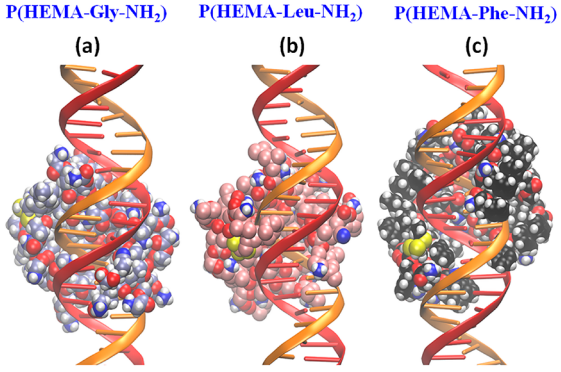

Figure 6. Molecular docking analysis of three different polymers: P(HEMA−Gly−NH_2) (a), P(HEMA−Leu−NH_2) (b), and P-(HEMA−Phe−NH_2) (c).

Table 2. Docking Results of Polymer−DNA Complex with DNA Sequence (Base Pair Length) Used for Docking, Actual Binding Sequence with Binding Affinity of Each Polymer

polymers	sequence	binding sequence	binding affinity (kcal/mol)	sequence	binding sequence	binding affinity (kcal/mol)
P(HEMA−Gly−NH_2)	48−250	CGCTGACTAATTTT	−2.6	3261−3304	CTGACTAATTGA	−2.7
P(HEMA−Leu−NH_2)	48−250	TCGCTGACTAATTT	−2.8	3261−3304	GACTAATTGAGA	−2.9
P(HEMA−Phe−NH_2)	48−250	TAATTTTTTTTATT	−2.9	3282−3323	AGCGGTGGTTTT	−3.5

DOI: 10.1021/acsabm.9b00639
ACS Appl. Bio Mater. 2019, 2, 5349−5365

Molecular Dynamics (MD). The polymer−DNA complex with the highest binding affinity was selected for molecular dynamics simulation. The root mean square deviation (RMSD) of each polymer and respective binding DNA are calculated from the MD trajectories, as depicted in Figure S9, Supporting Information. The RMSD indicates deviation of the molecule from the initial binding position. The RMSD trajectories of the polymers remained very stable throughout the MD simulation. The RMSD trajectory of P(HEMA−Leu−NH_2) has shown the least deviation followed by P(HEMA−Phe−NH_2). The RMSD of P(HEMA−Gly−NH_2) is observed to be very high compared to the others. The RMSD of DNA when bound with polymers is found to be high and fluctuating. It is due to the loose end of DNA, which is free to move. A change in the conformation of the polymer−DNA complex over a period of MD simulation is depicted in Figure 7. Both P(HEMA−Phe−NH_2) and P(HEMA−Leu−NH_2) have shown stable interactions, while P(HEMA−Leu−NH_2) started to loosen its hold on DNA as the MD simulation progressed. All the polymers have shown hydrogen bond, π−cation, and salt bridge interactions with DNA during MD simulation. The

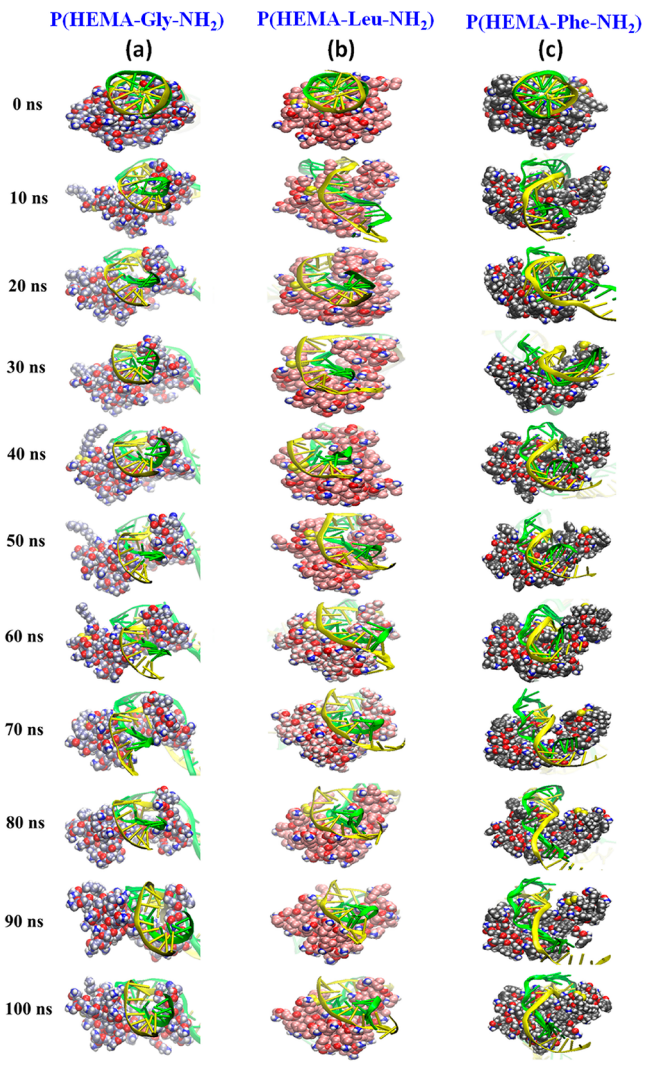

Figure 7. Snapshots of a molecular dynamics simulation study of P(HEMA−Gly−NH_2) (a), P(HEMA−Leu−NH_2) (b), and P-(HEMA−Phe−NH_2) (c) at different time points of 0, 10, 20, 30, 40, 50, 60 70, 80, 90, and 100 ns.

average Coulomb and van der Waal's interaction energy of each polymer with DNA are calculated using MD trajectories, as listed in Table 3. A lower interaction energy indicates a stable interaction by the polymers. In the case of P(HEMA−Phe−NH_2), both coulomb and vdW interaction energies are lowered compare to others. The RMSD trajectories, visual observation, and interaction energies indicate that complexes of P(HEMA−Phe−NH_2) and P(HEMA−Leu−NH_2) are more stable than P(HEMA−Gly−NH_2).

Table 3. Average Interaction Energy of Polymer with DNA Calculated from Trajectories Obtained from Molecular Dynamics

polymers	average coulomb energy (kcal)	average vdW energy (kcal)
P(HEMA−Gly−NH_2)	−66.11	−4.82
P(HEMA−Leu−NH_2)	−82.58	−4.37
P(HEMA−Phe−NH_2)	−81.96	−7.26

CD Spectra of Polymers and Polymer/pDNA Complexes. CD spectra help with understanding conformational changes in biomolecules. As observed in Figure 8, the typical CD spectra of the B form of pDNA exhibited a negative peak at 240−250 nm and a positive peak at 270−280 nm. The negative peak represents a helical structure, and the positive peak indicates a base pair stacking interaction of pDNA. It was observed in Figure 8d that P(HEMA−Leu−NH_2)/pDNA showed the highest deviation from the negative followed by the P(HEMA−Phe−NH_2)/pDNA and P(HEMA−Gly−NH_2)/pDNA complexes, indicating P(HEMA−Leu−NH_2)/pDNA and P(HEMA−Phe−NH_2)/pDNA complexes deviated from helical formation of pDNA more compared to the P(HEMA−Gly−NH_2)/pDNA complex. (However, in terms of degrees, the deviation is marginal.) The positive peak deviation was highest in the P(HEMA−Phe−NH_2)/pDNA complex compared to the other two polyplexes, suggesting a disturbance in the base pair stacking interaction during complexation. In Figure 8b,c, P(HEMA−Leu−NH_2) and P(HEMA−Phe−NH_2) before pDNA complexation individually showed a positive peak around 220−230 nm, indicating that the polymers were forming a secondary or helical structure due to intramolecular interaction. In Figure 8a, P(HEMA−Gly−NH_2) in the absence of pDNA did not show any positive peak like other polymers, which means that intramolecular interactions were low, and hence, P(HEMA−Gly−NH_2) could not arrange itself in a secondary structure. CD spectra at 0 and 10 min for P(HEMA−Gly−NH_2)/pDNA and P(HEMA−Leu−NH_2)/pDNA complexes (Figure 8a,b) exhibited similar patterns, indicating that no conformational changes occurred over period of 10 min. However, in Figure 8c, at 0 min, P(HEMA−Phe−NH_2)/pDNA showed significant conformational change around 240−250 nm but slowly settled and tried to get to its original conformation after 10 min. To conclude, CD spectra indicated a high amount of conformational change in P(HEMA−Leu−NH_2)/pDNA P(HEMA−Phe−NH_2)/pDNA complexes compared to the P(HEMA−Gly−NH_2)/pDNA complex because of the high binding affinity, which was also indicated by molecular docking and dynamics study. Henceforth, CD, molecular docking, and molecular dynamics study complement each other nicely.

DOI: 10.1021/acsabm.9b00639
ACS Appl. Bio Mater. 2019, 2, 5349−5365

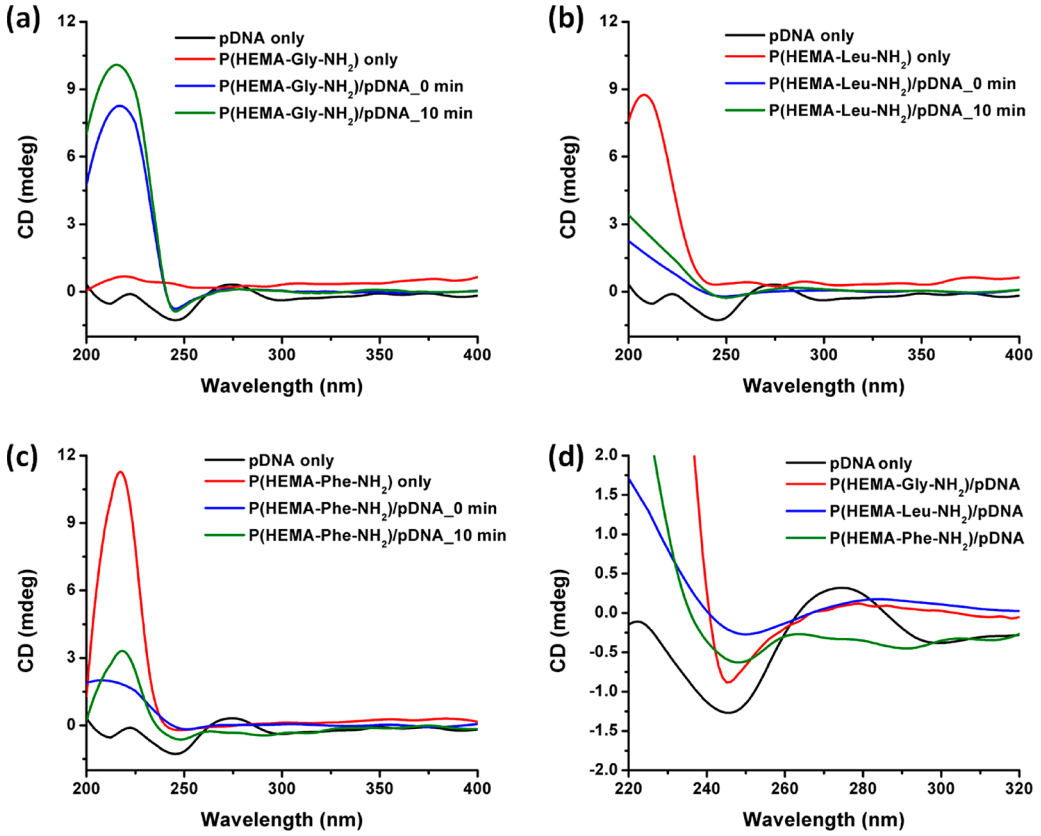

Figure 8. CD spectra of pDNA only, P(HEMA−Gly−NH_2) only, and the P(HEMA−Gly−NH_2)/pDNA complex at an N/P ratio of 100:1 after 0 and 10 min of complex formation (a), pDNA only, P(HEMA−Leu−NH_2) only, and the P(HEMA−Leu−NH_2)/pDNA complex at an N/P ratio of 100:1 after 0 and 10 min of complex formation (b), pDNA only, P(HEMA−Phe−NH_2) only, and the P(HEMA−Phe−NH_2)/pDNA complex at an N/P ratio of 100 after 0 and 10 min of complex formation (c), and pDNA only as well as the P(HEMA−Gly−NH_2)/pDNA, P(HEMA−Gly−NH_2)/pDNA, and P(HEMA−Gly−NH_2)/pDNA complexes at an N/P ratio of 100:1 after 10 min of complex formation (d).

Particle Size, Zeta Potential, and Morphology of Polymer/pDNA Complexes. The hydrodynamic particle size and zeta potential of polymer/DNA complexes (polyplexes) are important parameters that facilitate the cellular uptake through endocytosis and ultimately effect the transfection efficiency.[34,57] Therefore, the particle size and zeta potential of the polyplexes at different N/P ratios were measured, and corresponding values are represented in Table 4, Figure 9a−c, and Figures S10−S12, Supporting Information. The effect of pH on the particle size and zeta potential of the polyplexes was also determined, and the corresponding data are shown in Table 4. From Table 4, it is observed that P(HEMA−Phe−NH_2)/pDNA complexes showed smaller particle sizes among the other polyplexes at pH = 7.4. However, the particle sizes of all polyplexes were decreased at pH = 5.5. At a lower pH, the zeta potential might be increased significantly (although the zeta potential was not determined due to a higher conductivity value) through the protonation of primary amine groups and resulting smaller complexes through strong electrostatic interaction between the positively charged polymer and negatively charged pDNA. At pH = 7.4, the size of the P(HEMA−Gly−NH_2)/pDNA complexes was increased significantly, and it may be due to the aggregation effect of polyplexes offered by the higher positive zeta potential. Despite the almost similar zeta potentials of P(HEMA−Phe−NH_2)/pDNA polyplexes, the particle size did not change significantly. The presence of a phenyl group in the polymer backbone of P(HEMA−Phe−NH_2) might inhibit the aggregation effect through the hydrophobic−hydrophobic repulsion effect. The lesser binding capability of P(HEMA−Leu−NH_2) showed a larger hydrodynamic size of polyplexes at pH = 7.4. At basic pH, i.e., pH = 8.0, the negative zeta potential of P(HEMA−Gly−NH_2)/pDNA complexes again decreased the hydrodynamic size of the polyplexes due to a decrease of the aggregation effect. In comparison, the higher negative zeta potential of P(HEMA−Phe−NH_2)/pDNA polyplexes increased the hydrodynamic sizes because of a poor complexation capability with pDNA. From Figure 9a, it is found that the zeta potential of the P(HEMA−Gly−NH_2)/pDNA complex at pH = 7.4 changed from a negative zeta potential (−3.3 ± 2 mV) at an N/P ratio of 1 to a positive zeta potential (+23 ± 3 mV) at an N/P ratio of 5, which indicates the formation of polyplex through neutralizing the all negative charges of pDNA, and the overall positive zeta potential resulted in the retardation of the electrophoretic mobility of pDNA as shown in Figure 5a. In comparison, P(HEMA−Leu−NH_2)/pDNA and P(HEMA−Phe−NH_2)/pDNA complexes showed a positive zeta potential at N/P ratios of 60 (Figure 9b) and 10 (Figure 9c), respectively. It is noticed that the positive zeta potential value gradually increased with an increase in the N/P ratios and plateaued after a particular N/P ratio, which indicates the complete complexation of all pDNA by the polymer chain. The plateau was observed for P(HEMA−Gly−NH_2)/pDNA, P(HEMA−Leu−NH_2)/pDNA, and P(HEMA−Phe−NH_2)/pDNA complexes at N/P ratios of 10:1, 80:1, and 40:1, respectively, which corroborated

DOI: 10.1021/acsabm.9b00639
ACS Appl. Bio Mater. 2019, 2, 5349−5365

Table 4. Particle Size, Polydispersity Index (PDI), and Zeta Potential (ZP) of P(HEMA−Gly−NH_2)/pDNA, P(HEMA−Leu−NH_2)/pDNA, and P(HEMA−Phe−NH_2)/pDNA Complexes at the N/P Ratios of 0, 5, 10, 20, 40, 60, 80, and 100 at different pHs of pH= 5.5, 7.4, and 8.0

	P(HEMA−Gly−NH_2)			P(HEMA−Leu−NH_2)			P(HEMA−Phe−NH_2)		
N/P ratio	size[a] (nm)	PDI[a]	ZP[a] (mV)	size[a] (nm)	PDI[a]	ZP[a] (mV)	size[a] (nm)	PDI[a]	ZP[a] (mV)
pH = 5.5									
0	412 ± 36	0.75 ± 0.1	−3 ± 3	412 ± 36	0.75 ± 0.1	−3 ± 3	412 ± 36	0.75 ± 0.1	−3 ± 3
2	246 ± 61	0.56 ± 0.1	NR	147 ± 43	0.38 ± 0.1	NR	103 ± 6	0.33 ± 0.1	NR
10	251 ± 73	0.61 ± 0.2	NR	187 ± 5	0.47 ± 0.1	NR	86 ± 10	0.38 ± 0.1	NR
20	224 ± 5	0.54 ± 0.1	NR	176 ± 27	0.55 ± 0.2	NR	80 ± 40	0.33 ± 0.1	NR
40	241 ± 34	0.51 ± 0.1	NR	191 ± 76	0.38 ± 0.1	NR	112 ± 75	0.34 ± 0.2	NR
60	179 ± 142	0.76 ± 0.2	NR	192 ± 76	0.51 ± 0.1	NR	136 ± 71	0.38 ± 0.1	NR
80	198 ± 49	0.56 ± 0.1	NR	231 ± 6	0.58 ± 0.1	NR	208 ± 69	0.42 ± 0.1	NR
100	232 ± 49	0.66 ± 0.2	NR	152 ± 55	0.45 ± 0.1	NR	116 ± 58	0.39 ± 0.1	NR
pH = 7.4									
0	209 ± 9	0.37 ± 0.1	−22 ± 3	209 ± 9	0.37 ± 0.1	−22 ± 3	209 ± 9	0.37 ± 0.1	−22 ± 3
5	711 ± 56	0.87 ± 0.1	+23 ± 2	335 ± 6	0.34 ± 0.1	−24 ± 3	620 ± 90	0.80 ± 0.1	−6 ± 1
10	379 ± 14	0.33 ± 0.1	+28 ± 2	455 ± 14	0.24 ± 0.1	−28 ± 3	509 ± 55	0.65 ± 0.1	+14 ± 3
20	606 ± 50	0.41 ± 0.1	+26 ± 2	574 ± 18	0.33 ± 0.1	−5 ± 2	499 ± 27	0.53 ± 0.1	+30 ± 1
40	556 ± 36	0.38 ± 0.1	+27 ± 3	750 ± 16	0.27 ± 0.1	−3 ± 1	547 ± 63	0.59 ± 0.2	+25 ± 1
60	625 ± 15	0.49 ± 0.1	+33 ± 3	828 ± 31	0.24 ± 0.1	+9 ± 3	345 ± 19	0.31 ± 0.1	+27 ± 3
80	644 ± 50	0.47 ± 0.1	+30 ± 3	963 ± 40	0.31 ± 0.1	+21 ± 3	335 ± 10	0.33 ± 0.1	+33 ± 4
100	707 ± 41	0.53 ± 0.1	+30 ± 2	977 ± 31	0.21 ± 0.1	+16 ± 3	470 ± 54	0.33 ± 0.1	+28 ± 4
pH = 8.0									
0	995 ± 60	0.92 ± 0.1	−6 ± 4	995 ± 60	0.92 ± 0.1	−6 ± 4	995 ± 60	0.92 ± 0.1	−6 ± 4
5	739 ± 163	0.79 ± 0.1	−10 ± 3	333 ± 81	0.64 ± 0.1	−7 ± 3	439 ± 18	0.48 ± 0.1	−7 ± 2
10	400 ± 39	0.58 ± 0.1	−7 ± 2	151 ± 2	0.44 ± 0.1	−6 ± 1	875 ± 58	0.52 ± 0.2	−13 ± 2
20	401 ± 36	0.57 ± 0.1	−8 ± 2	169 ± 2	0.23 ± 0.1	−6 ± 1	723 ± 17	0.57 ± 0.1	−19 ± 3
40	329 ± 3	0.38 ± 0.1	−5 ± 4	215 ± 1	0.20 ± 0.1	−13 ± 4	534 ± 87	0.60 ± 0.1	−12 ± 3
60	351 ± 24	0.42 ± 0.1	−5 ± 2	268 ± 4	0.20 ± 0.1	−25 ± 2	339 ± 38	0.30 ± 0.1	−5 ± 3
80	371 ± 9	0.32 ± 0.1	−5 ± 3	280 ± 0.5	0.18 ± 0.1	−25 ± 2	637 ± 24	0.95 ± 0.1	−25 ± 4
100	401 ± 6	0.31 ± 0.1	−5 ± 1	318 ± 4	0.26 ± 0.1	−25 ± 3	356 ± 9	0.28 ± 0.1	−25 ± 14

[a]Measured by DLS using Zetasizer NanoZS (Malvern) at pH = 5.5, 7.4, and 8.0. NR: No result (at pH = 5.5, all the polyplexes showed very high conductivity (>8 ms/cm), which is not measurable by the instrument).

well with the retardation of electrophoretic mobility of pDNA as shown in Figure 5.

The pDNA loading efficiency in polyplexes at pH = 7.4 was also calculated, and the corresponding data are shown in Table 5. As a result of the better DNA complexation capability of P(HEMA−Gly−NH_2) compared to P(HEMA−Leu−NH_2) and P(HEMA−Phe−NH_2) as shown in the agarose gel electrophoresis assay (Figure 5), P(HEMA−Gly−NH_2) showed the highest DNA loading efficiency, and more than 95% pDNA was loaded in the complex at higher N/P ratios, whereas P(HEMA−Leu−NH_2) and P(HEMA−Phe−NH_2) showed almost similar pDNA loading efficiencies.

The morphology of the gene carrier system plays an important role on cellular uptake, the endocytosis mechanism which affects the transfection efficiency.[55,58] Therefore, we observed the morphology of all polymer/pDNA complexes at an N/P ratio of 100 by TEM, and the corresponding images are shown in Figure 9d−f. From Figure 9d−f, it is observed that both the polymers P(HEMA−Gly−NH_2) (Figure 9d) and P(HEMA−Leu−NH_2) (Figure 9e) formed spherical shaped nanocomplexes at an N/P ratio of 100, whereas interestingly P(HEMA−Phe−NH_2) formed a hexagonal shaped nanocomplex at the same N/P ratio (Figure 9f). Among all the polymers, P(HEMA−Gly−NH_2) formed smaller complexes with pDNA having a particle size around 120−150 nm. In contrast, P(HEMA−Leu−NH_2) and P(HEMA−Phe−NH_2) formed comparatively larger nanocomplexes with pDNA with particle sizes of 200−250 and 400−450 nm, respectively.

The stability of the polyplexes formed by pDNA and polymers such as P(HEMA−Gly−NH_2), P(HEMA−Leu−NH_2), and P(HEMA−Phe−NH_2) was studied in the presence of DMEM media containing serum (10% FBS) and serum-free DMEM medium. This study is significant in order to understand how the polymer structure affects the polyplex stability during complexation. As shown in Figure S13, Supporting Information, in complete DMEM (10% FBS), the P(HEMA−Gly−NH_2)/pDNA complex exhibited the smallest particle size (39 ± 1 to 45 ± 3 nm) followed by P(HEMA−Leu−NH_2)/pDNA (73 ± 1 to 76 ± 2 nm) and P(HEMA−Phe−NH_2)/pDNA (91 ± 1 to 97 ± 1 nm). It is noteworthy that in serum-containing media, the particle size of the polyplexes did not alter much with incubation time, which means the polyplexes remained invariably stable in FBS-supplemented DMEM (Figure S13a, Supporting Information). Pezzoli et al. also observed the same thing while the presence of FBS blunted the aggregation of polyplexes, which was reflected by the modest increase of the hydrodynamic diameter of the polyplexes by 50−100 nm within the first few minutes of incubation and then subsequent stabilization.[59] They had explained that this behavior might be due to the prompt adsorption of serum proteins onto polyplexes, which resulted in a small initial increase in hydrodynamic diameter, but with further increasing incubation time, long-term aggregation was

DOI: 10.1021/acsabm.9b00639
ACS Appl. Bio Mater. 2019, 2, 5349−5365

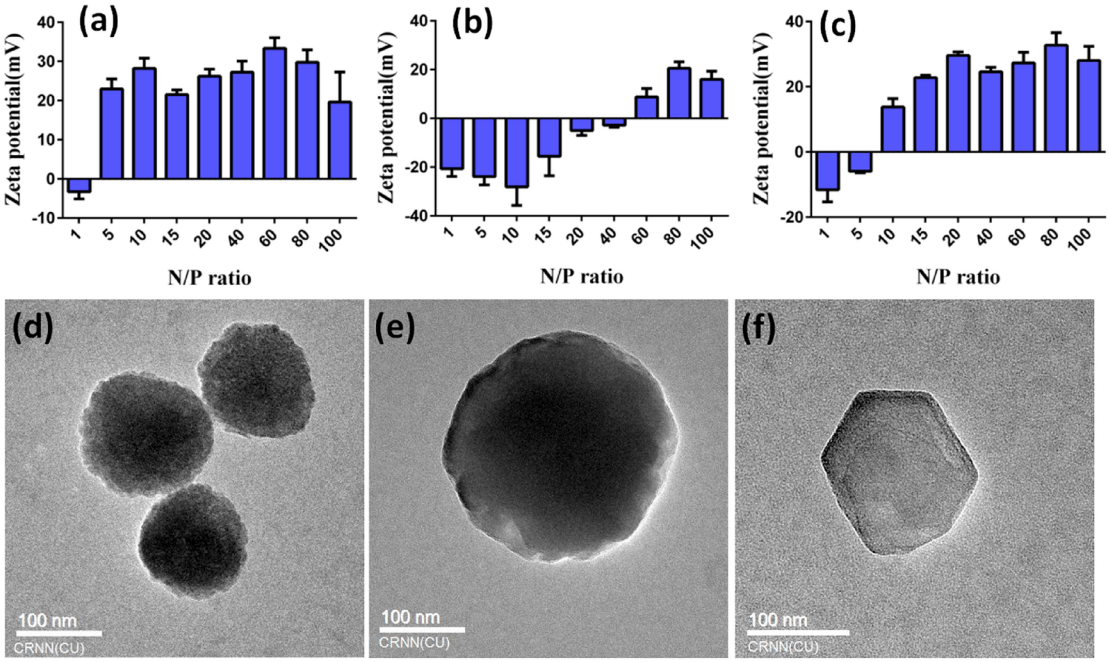

Figure 9. Zeta potential of P(HEMA−Gly−NH_2)/pDNA (a), P(HEMA−Leu−NH_2)/pDNA (b), and P(HEMA−Phe−NH_2)/pDNA complexes (c) at different N/P ratios of 0:1, 1:1, 5:1, 10:1, 15:1, 20:1, 40:1, 60:1, 80:1, and 100:1. In each N/P ratio, 1 μg of pDNA was used during the complex formation. TEM images of the P(HEMA−Gly−NH_2)/pDNA complex (d), P(HEMA−Leu−NH_2)/pDNA complex (e), and P(HEMA−Phe−NH_2)/pDNA complex (f) at an N/P ratio of 100:1.

Table 5. pDNA Loading Efficiency (%) in P(HEMA−Gly−NH_2)/pDNA, P(HEMA−Leu−NH_2)/pDNA, and P(HEMA−Phe−NH_2)/pDNA Complexes at Different N/P Ratios of 0, 5:1, 10:1, 20:1, 40:1, 60:1, 80:1, 100:1, 150:1, and 200:1

	P(HEMA−Gly−NH_2)	P(HEMA−Leu−NH_2)	P(HEMA−Phe−NH_2)
N/P ratio	pDNA loading in polyplex[a] (%)	pDNA loading in polyplex[a] (%)	pDNA loading in polyplex[a] (%)
0	0	0	0
1	82 ± 3	80 ± 2	78 ± 3
5	93 ± 2	79 ± 3	96 ± 1
10	97 ± 1	80 ± 2	94 ± 1
15	98 ± 1	79 ± 3	93 ± 1
20	98 ± 1	73 ± 3	88 ± 2
40	96 ± 2	83 ± 2	80 ± 3
60	98 ± 1	86 ± 2	80 ± 3
80	99 ± 1	88 ± 1	70 ± 3
100	96 ± 2	68 ± 3	68 ± 2
150	97 ± 2	65 ± 3	65 ± 2
200	99 ± 1	69 ± 3	69 ± 2

[a]Measured by Nanodrop, Thermo Scientific, 2000/2000C.

prevented by reducing particle−particle interactions. Therefore, we also hypothesized that in complete DMEM, the presence of serum prevented the aggregation of polyplexes, thus keeping them stable over time.

In contrast to what we observed in serum-supplemented media, upon dilution in serum-free medium, the size of P(HEMA−Leu−NH_2)/pDNA and P(HEMA−Phe−NH_2)/pDNA complexes enhanced over time from 50 ± 3 to 70 ± 5 nm, while the particle size of the P(HEMA−Gly−NH_2)/pDNA complex at first increased and then decreased with time (Figure S13b, Supporting Information), which can be explained by the irreversible aggregation of polyplexes with time. Of note, the larger the dimensions of the polyplexes (in the nano- to micrometer range), the higher and faster the sedimentation rate and therefore the greater their efficiency in vitro.[59] Therefore, the larger particle size of the P(HEMA−Phe−NH_2)/pDNA complex when compared to other two polyplexes might also play a key role towards a promising transfection efficiency with the P(HEMA−Phe−NH_2) polymer.

Resistance of Polymer/pDNA Complexes against Anionic Surfactants and Enzyme. For successful in vivo gene therapy, the carrier/DNA complex should be stable in body fluid, as it consists of lots of negatively charged protein and enzymes. Therefore, we characterized the stability of the polymer/pDNA complexes against the negatively charged heparin and DNase I as model protein and enzyme, respectively, and the corresponding results are shown in Figures S14 and S15, Supporting Information, respectively. The stability of the polyplexes toward anionic surfactant was further investigated by heparin, as it is more physiological than SDS. As shown in Figure S14, Supporting Information, P(HEMA−Gly−NH_2) was able to protect pDNA against decomplexation in the presence of heparin, at a concentration of 0.05 mg/mL, and beyond this concentration, the pDNA started decomplexation from the polyplex through electrostatic repulsion between heparin and pDNA. In contrast, P(HEMA−Leu−NH_2)/pDNA and P(HEMA−Phe−NH_2)/pDNA complexes were disrupted at comparatively lower heparin concentrations of 0.01 mg/mL (Figure S14b,c, Supporting Information). This result is a reflection of the agarose gel electrophoresis assay (Figure 5), where P(HEMA−Gly−NH_2) showed better complexation and hence resulted in better protection of pDNA against the anionic moiety.

Figure S15, Supporting Information shows the DNase I assay of polymers/pDNA complexes in the presence of DNase

DOI: 10.1021/acsabm.9b00639
ACS Appl. Bio Mater. 2019, 2, 5349−5365

I enzyme. The first lane of Figure S15a, Supporting Information shows the DNA digestion activity of DNase I where naked pDNA was completely digested and resulted in the complete disappearance of DNA band. It is observed from Figure S15a, Supporting Information that P(HEMA−Gly−NH_2) completely protected pDNA against DNase I digestion at an N/P ratio of 20:1, whereas P(HEMA−Leu−NH_2) and P(HEMA−Phe−NH_2) showed complete protection at a slightly higher N/P ratio of 40:1. The higher DNA complexation capability of P(HEMA−Gly−NH_2) showed better pDNA protection against enzyme digestion compared to P(HEMA−Leu−NH_2) and P(HEMA−Phe−NH_2). However, all the polymers showed complete protection of pDNA against enzyme digestion at a higher N/P ratio of 100, at which higher transfection efficiency was observed. Therefore, the polymers/pDNA complexes at a higher N/P ratio may give better transfection efficiency in vivo also.

Intracellular Uptake Kinetics. As the morphology of the nanoparticle has an effect on cellular uptake, we measured the intracellular uptake kinetics using the FITC conjugated polymer/pDNA (PGL3 control vector was used) complexes at an N/P ratio of 100 with different time intervals such as 0.5, 2.0, and 4.0 h, and the corresponding confocal images are shown in Figure 10. The P(HEMA−Gly−NH_2)/pDNA

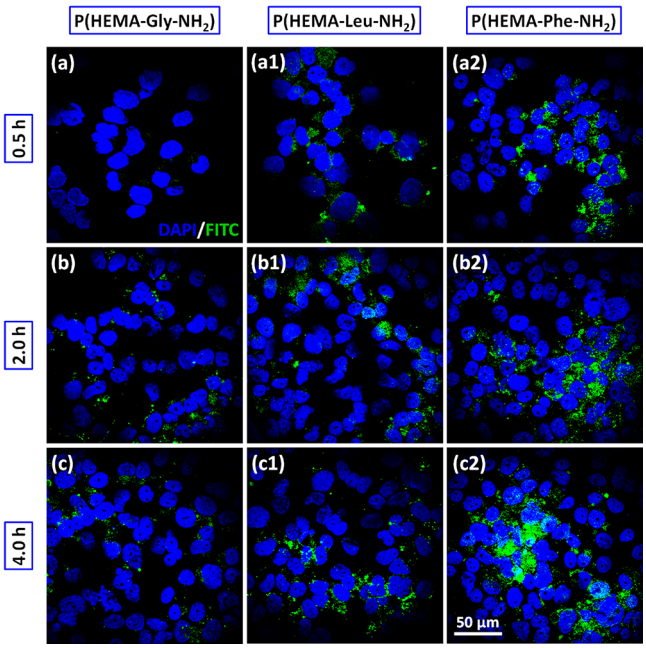

Figure 10. Representative fluorescence images of the intracellular kinetics of the cellular uptake of FITC conjugated P(HEMA−Gly−NH_2)/pDNA complex (a−c), P(HEMA−Leu−NH_2)/pDNA complex (a1−c1), and P(HEMA−Phe−NH_2)/pDNA complex (a2−c2) at the predetermined time intervals of 0.5, 2, and 4 h at an N/P ratio of 100:1 against MDA-MB-231 cells.

complex showed the lowest cellular uptake (Figure 10a−c) compared to that of other two polymers. In contrast, the cellular uptake of the P(HEMA−Phe−NH_2)/pDNA complex was significantly higher, although the cellular uptake was time dependent (Figure 10a2−c2). The hexagonal morphology of the P(HEMA−Phe−NH_2)/pDNA complex might better help cellular uptake compared to the spherical shaped morphology of both the P(HEMA−Gly−NH_2)/pDNA and P(HEMA−Leu−NH_2)/pDNA complexes. In a recent study, Lunnoo et al. showed the effect of the nanoparticle shape, size, charge, and aggregation on cellular uptake by coarse-grained MD simulations.[60] They observed that the aggregated nanoparticles slowed down the cellular uptake compared with nonaggregated nanoparticles. The smaller particle size (around 120−150 nm) of P(HEMA−Gly−NH_2)/pDNA complexes might help to form aggregation because of the higher surface activation charge and resulting lowest cellular uptake after 4 h of cellular uptake kinetic study (Figure 10c). Lunnoo et al. also noticed that the hexagonal shaped nanoparticle (nanohexapoid) possessed the lowest free energy barrier (ΔG = 80.25 ± 5.75 kJ/mol) and consequently showed the highest cellular uptake compared to those of the nanosphere (ΔG = 260.85 ± 6.04 kJ/mol), nanocage (ΔG = 443.97 ± 40.34 kJ/mol), nanorod (ΔG = 310.56 ± 8.91 kJ/mol), and nanoplate (ΔG = 321.16 ± 5.81 kJ/mol). Therefore, we also hypothesized that the hexagonal shaped P(HEMA−Phe−NH_2)/pDNA complex showed a higher cellular uptake because of the lower free energy barrier compared to that of the spherical shaped P(HEMA−Gly−NH_2)/pDNA and P(HEMA−Leu−NH_2)/pDNA complexes, and the phenomenon is schematically shown in Figure 11.

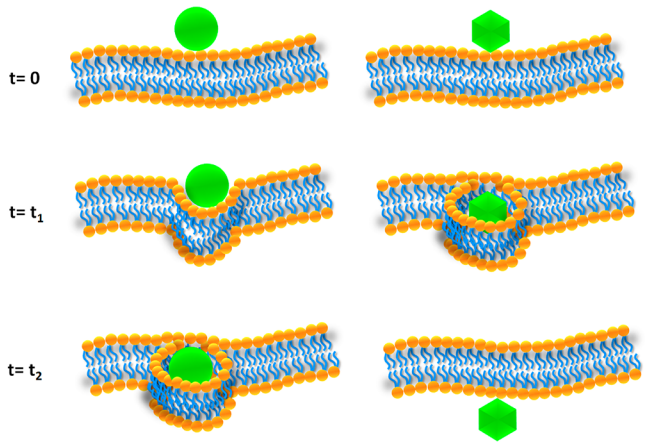

Figure 11. Schematic representation of the cellular uptake kinetics of spherical shaped and hexagonal shaped nanoparticles through the cellular membrane.

In Vitro Transfection Efficiency. The transfection efficiency of all polymers/pDNA complexes at the N/P ratios of 10, 50, and 100 was investigated on MDA-MB-231 cells by using pDNA encoded with the enhanced green fluorescence protein (eGFP) gene. Poor green fluorescence was observed for all polymers at low N/P ratios of 10 and 50 (data not shown), but the green fluorescence intensity significantly increased at the N/P ratio of 100 for all polymers as shown in Figure 12A, a−c. Incomplete pDNA complexation at a low N/P ratio might result in the poor transfection efficiency. Interestingly, it is observed that the polymer P(HEMA−Phe−NH_2) showed superior transfection efficiency as shown in Figure 12A, c where overexpression of green fluorescence was observed compared to P(HEMA−Gly−NH_2) and P(HEMA−Leu−NH_2). In comparison, the transfection efficiency of P(HEMA−Phe−NH_2) was also higher than that of LF2K (Figure 12A, g). The transfection efficiency was further quantified by FACS, and the corresponding data are shown in Figure 12B. From Figure 12B, it is found that the transfection efficiency of P(HEMA−Phe−NH_2) was signifi-

DOI: 10.1021/acsabm.9b00639
ACS Appl. Bio Mater. 2019, 2, 5349−5365

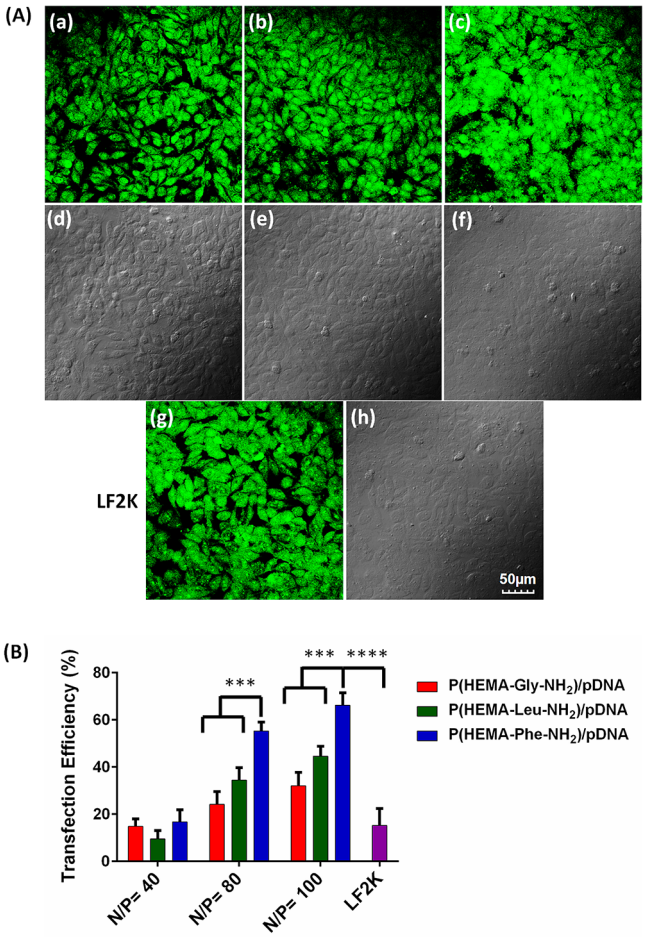

Figure 12. Green fluorescence confocal images of the in vitro transfection efficiency (A) by the P(HEMA−Gly−NH_2)/pDNA complex (a), P(HEMA−Leu−NH_2)/pDNA complex (b), and P(HEMA−Phe−NH_2)/pDNA complex (c) at an N/P ratio of 100:1 and their corresponding bright field images (d−f). The represented confocal images of transfected cells by the LF2K/pDNA complex (g) and its corresponding bright field image (h). The quantification of the transfection efficiency by FACS analysis (B) of P(HEMA−Gly−NH_2)/pDNA, P(HEMA−Leu−NH_2)/pDNA, and P(HEMA−Phe−NH_2)/pDNA complexes at N/P ratios of 40:1, 80:1, and 100:1. LF2K was used as a positive control.

cantly higher at N/P ratios of 80:1 and 100:1 compared to that of both P(HEMA−Gly−NH_2) and P(HEMA−Leu−NH_2), and the highest transfection efficiency of the P(HEMA−Phe−NH_2)/pDNA complex at an N/P ratio of 100:1 was obtained around 72%, which was much higher than that of LF2K. The higher cellular uptake of the P(HEMA−Phe−NH_2)/pDNA complex due to its unique hexagonal morphology might result in a higher transfection efficiency. Previously, it was also observed that an oval shaped nanoparticle showed a higher transfection efficiency compared to that of the spherical shaped nanoparticle.[55,61]

CONCLUSION

In this present work, we synthesized three different amino acid based gene delivery vectors through RAFT polymerization, adopting a similar synthetic strategy. All polymers showed very low toxicity against both cancerous and normal cells even at a higher concentration of 1000 μg/mL. In addition to this, the polymers also showed blood compatibility with negligible hemolysis at slightly lower concentration of 500 μg/mL. All polymers showed excellent pDNA complexation capability, better resistance toward anionic surfactant, and also appreciable gene protection capability against enzymatic degradation, although it was dependent on the N/P ratio. Interestingly, P(HEMA−Phe−NH_2) formed a unique hexagonal shaped nanoparticle through complexation with pDNA, whereas other polymers formed spherical shaped nanoparticles. The hexagonal morphology of the P(HEMA−Phe−NH_2)/pDNA complex significantly improved the cellular uptake through endocytosis and resulted in a superior transfection efficiency against triple negative breast cancer. Therefore, these polymers may constitute a promising gene carrier system in gene therapy in the future.

ASSOCIATED CONTENT

Supporting Information

The Supporting Information is available free of charge on the ACS Publications website at DOI: 10.1021/acsabm.9b00639.

Characterization of monomers by FTIR, ^{1}H NMR, and ^{13}C NMR, characterization of RAFT reagent CDP by DSC, FTIR, and ^{1}H NMR, characterization of polymers by FTIR and ^{1}H NMR, RMSD calculation from molecular dynamics trajectories, determination of zeta potential of polymer/pDNA complexes by Zetasizer Nano ZS, observation of particle size (hydrodynamic size) of polymer/pDNA complexes in presence and absence of serum by DLS, and stability of polymer/pDNA complexes against heparin and DNase I by agarose gel electrophoresis assay (PDF)

AUTHOR INFORMATION

Corresponding Author

*E-mail: kishorpst@gmail.com or kspoly@caluniv.ac.in; Phone: +91-33-2350-1397 (Ext: 285); Website: www.kishorgttl.com.

ORCID

Sagar Bhayye: 0000-0001-7441-8045

Kishor Sarkar: 0000-0002-1451-426X

Notes

The authors declare no competing financial interest.

ACKNOWLEDGMENTS

This work is financially supported by the DST-SERB funding agency through two sanctioned projects *EEQ/2016/000712* and *ECR/2016/002018*. K.S. and R.S. also acknowledge UGC for the UGC-BSR Research Start-Up Grant (F.30-363/2017(BSR), Dt- 08/08/2017) and CU for the UPE-II Nanofabrication project fund (UGC/166/UPE-II, Dt- 03/04/2017) for financial support. The authors acknowledge Prof. Dilip Kumar Maiti (Professor, Department of Chemistry, University of Calcutta) for providing the dynamic light scattering (DLS) instrument and Dr. Kuldip Jana (Principal Scientist, Division of molecular medicine, Bose Institute, Kolkata) for providing the Circular Dichroism (CD) spectrometer.

REFERENCES

(1) Liu, L.; Wang, Y.; Miao, L.; Liu, Q.; Musetti, S.; Li, J.; Huang, L. Combination immunotherapy of MUC1 mRNA nano-vaccine and CTLA-4 blockade effectively inhibits growth of triple negative breast cancer. *Mol. Ther.* **2018**, *26* (1), 45−55.

DOI: 10.1021/acsabm.9b00639
ACS Appl. Bio Mater. 2019, 2, 5349−5365

(2) Foulkes, W. D.; Smith, I. E.; Reis-Filho, J. S. Triple-negative breast cancer. *N. Engl. J. Med.* **2010**, *363* (20), 1938−1948.
(3) O'toole, S. A.; Beith, J. M.; Millar, E. K.; West, R.; McLean, A.; Cazet, A.; Swarbrick, A.; Oakes, S. R. Therapeutic targets in triple negative breast cancer. *J. Clin. Pathol.* **2013**, *66* (6), 530−542.
(4) Metzger-Filho, O.; Tutt, A.; De Azambuja, E.; Saini, K. S.; Viale, G.; Loi, S.; Bradbury, I.; Bliss, J. M.; Azim, H. A., Jr; Ellis, P.; et al. Dissecting the heterogeneity of triple-negative breast cancer. *J. Clin. Oncol.* **2012**, *30* (15), 1879−1887.
(5) Turner, N.; Moretti, E.; Siclari, O.; Migliaccio, I.; Santarpia, L.; D'Incalci, M.; Piccolo, S.; Veronesi, A.; Zambelli, A.; Del Sal, G.; et al. Targeting triple negative breast cancer: is p53 the answer? *Cancer Treat. Rev.* **2013**, *39* (5), 541−550.
(6) Duffy, M. J.; McGowan, P. M.; Crown, J. Targeted therapy for triple-negative breast cancer: Where are we? *Int. J. Cancer* **2012**, *131* (11), 2471−2477.
(7) Kuo, S.-H.; Lien, H.-C.; You, S.-L.; Lu, Y.-S.; Lin, C.-H.; Chen, T.-Z.; Huang, C.-S. Dose variation and regimen modification of adjuvant chemotherapy in daily practice affect survival of stage I−II and operable stage III Taiwanese breast cancer patients. *Breast* **2008**, *17* (6), 646−653.
(8) Denyer, R.; Douglas, M. R. Gene therapy for Parkinson's disease. *Parkinson's Dis.* **2012**, *2012*, 757305.
(9) Dishart, K. L.; Work, L. M.; Denby, L.; Baker, A. H. Gene therapy for cardiovascular disease. *J. Biomed. Biotechnol.* **2003**, *2003* (2), 138−148.
(10) Osta, W. A.; Chen, Y.; Mikhitarian, K.; Mitas, M.; Salem, M.; Hannun, Y. A.; Cole, D. J.; Gillanders, W. E. EpCAM is overexpressed in breast cancer and is a potential target for breast cancer gene therapy. *Cancer Res.* **2004**, *64* (16), 5818−5824.
(11) Mesri, M.; Wall, N. R.; Li, J.; Kim, R. W.; Altieri, D. C. Cancer gene therapy using a survivin mutant adenovirus. *J. Clin. Invest.* **2001**, *108* (7), 981−990.
(12) Lungwitz, U.; Breunig, M.; Blunk, T.; Göpferich, A. Polyethylenimine-based non-viral gene delivery systems. *Eur. J. Pharm. Biopharm.* **2005**, *60* (2), 247−266.
(13) Zhang, Z.; Shen, W.; Ling, J.; Yan, Y.; Hu, J.; Cheng, Y. The fluorination effect of fluoroamphiphiles in cytosolic protein delivery. *Nat. Commun.* **2018**, *9* (1), 1377.
(14) Choi, J. S.; Nam, K.; Park, J.-y.; Kim, J.-B.; Lee, J.-K.; Park, J.-s. Enhanced transfection efficiency of PAMAM dendrimer by surface modification with L-arginine. *J. Controlled Release* **2004**, *99* (3), 445−456.
(15) Eichman, J. D.; Bielinska, A. U.; Kukowska-Latallo, J. F.; Baker, J. R., Jr The use of PAMAM dendrimers in the efficient transfer of genetic material into cells. *Pharm. Sci. Technol. Today* **2000**, *3* (7), 232−245.
(16) Wang, M.; Liu, H.; Li, L.; Cheng, Y. A fluorinated dendrimer achieves excellent gene transfection efficacy at extremely low nitrogen to phosphorus ratios. *Nat. Commun.* **2014**, *5*, 3053.
(17) Wang, H.; Wang, Y.; Wang, Y.; Hu, J.; Li, T.; Liu, H.; Zhang, Q.; Cheng, Y. Self-Assembled Fluorodendrimers Combine the Features of Lipid and Polymeric Vectors in Gene Delivery. *Angew. Chem., Int. Ed.* **2015**, *54* (40), 11647−11651.
(18) Cheng, Y. Fluorinated polymer gene carrier. *Acta Polym. Sin.* **2017**, *8* (8), 1234−1245.
(19) Ghosal, K.; Sarkar, K. Biomedical Applications of Graphene Nanomaterials and Beyond. *ACS Biomater. Sci. Eng.* **2018**, *4* (8), 2653−2703.
(20) Sarkar, K.; Chatterjee, A.; Chakraborti, G.; Kundu, P. P. Blood compatible N-maleyl chitosan-graft-PAMAM copolymer for enhanced gene transfection. *Carbohydr. Polym.* **2013**, *98* (1), 596−606.
(21) Erbacher, P.; Zou, S.; Bettinger, T.; Steffan, A.-M.; Remy, J.-S. Chitosan-based vector/DNA complexes for gene delivery: biophysical characteristics and transfection ability. *Pharm. Res.* **1998**, *15* (9), 1332−1339.
(22) Thomas, C. E.; Ehrhardt, A.; Kay, M. A. Progress and problems with the use of viral vectors for gene therapy. *Nat. Rev. Genet.* **2003**, *4*, 346.
(23) Robbins, P. D.; Ghivizzani, S. C. Viral vectors for gene therapy. *Pharmacol. Ther.* **1998**, *80* (1), 35−47.
(24) Ghosal, K.; Ghosh, A. Carbon dots: The next generation platform for biomedical applications. *Mater. Sci. Eng., C* **2019**, *96*, 887−903.
(25) Gargouri, M.; Sapin, A.; Bouali, S.; Becuwe, P.; Merlin, J.; Maincent, P. Optimization of a new non-viral vector for transfection: Eudragit nanoparticles for the delivery of a DNA plasmid. *Technol. Cancer Res. Treat.* **2009**, *8* (6), 433−443.
(26) Castillo-Rodríguez, R. A.; Arango-Rodríguez, M. L.; Escobedo, L.; Hernandez-Baltazar, D.; Gompel, A.; Forgez, P.; Martínez-Fong, D. Suicide HSVtk gene delivery by neurotensin-polyplex nanoparticles via the bloodstream and GCV Treatment specifically inhibit the growth of human MDA-MB-231 triple negative breast cancer tumors xenografted in athymic mice. *PLoS One* **2014**, *9* (5), No. e97151.
(27) Deming, T. J. Methodologies for preparation of synthetic block copolypeptides: materials with future promise in drug delivery. *Adv. Drug Delivery Rev.* **2002**, *54* (8), 1145−1155.
(28) Nowak, A. P.; Breedveld, V.; Pakstis, L.; Ozbas, B.; Pine, D. J.; Pochan, D.; Deming, T. J. Rapidly recovering hydrogel scaffolds from self-assembling diblock copolypeptide amphiphiles. *Nature* **2002**, *417* (6887), 424.
(29) Chécot, F.; Lecommandoux, S.; Gnanou, Y.; Klok, H. A. Water-soluble stimuli-responsive vesicles from peptide-based diblock copolymers. *Angew. Chem., Int. Ed.* **2002**, *41* (8), 1339−1343.
(30) Moad, G.; Rizzardo, E.; Thang, S. H. Living radical polymerization by the RAFT process. *Aust. J. Chem.* **2005**, *58* (6), 379−410.
(31) Moad, G.; Chong, Y.; Postma, A.; Rizzardo, E.; Thang, S. H. Advances in RAFT polymerization: the synthesis of polymers with defined end-groups. *Polymer* **2005**, *46* (19), 8458−8468.
(32) Sun, H.; Gao, C. Facile synthesis of multiamino vinyl poly (amino acid) s for promising bioapplications. *Biomacromolecules* **2010**, *11* (12), 3609−3616.
(33) Kumar, S.; Roy, S. G.; De, P. Cationic methacrylate polymers containing chiral amino acid moieties: controlled synthesis via RAFT polymerization. *Polym. Chem.* **2012**, *3* (5), 1239−1248.
(34) Sarkar, K.; Madras, G.; Chatterjee, K. Dendron conjugation to graphene oxide using click chemistry for efficient gene delivery. *RSC Adv.* **2015**, *5* (62), 50196−50211.
(35) Sarkar, K.; Kundu, P. Preparation of low molecular weight N-maleated chitosan-graft-PAMAM copolymer for enhanced DNA complexation. *Int. J. Biol. Macromol.* **2012**, *51* (5), 859−867.
(36) Sarkar, K.; Kundu, P. PAMAM conjugated chitosan through naphthalimide moiety for enhanced gene transfection efficiency. *Carbohydr. Polym.* **2013**, *98* (1), 495−504.
(37) Ghosh, S.; Ghosal, K.; Mohammad, S. A.; Sarkar, K. Dendrimer functionalized carbon quantum dot for selective detection of breast cancer and gene therapy. *Chem. Eng. J.* **2019**, *373*, 468−484.
(38) Sarkar, K.; Kundu, P. P. Preparation of low molecular weight N-maleated chitosan-graft-PAMAM copolymer for enhanced DNA complexation. *Int. J. Biol. Macromol.* **2012**, *51* (5), 859−867.
(39) Dagani, R. Nanomaterials: Safe or Unsafe? *Chem. Eng. News* **2003**, *81*, 30.
(40) Pettersen, E. F.; Goddard, T. D.; Huang, C. C.; Couch, G. S.; Greenblatt, D. M.; Meng, E. C.; Ferrin, T. E. UCSF Chimera—a visualization system for exploratory research and analysis. *J. Comput. Chem.* **2004**, *25* (13), 1605−1612.
(41) Santos, J. d. O.; Pereira, G. R.; Brandão, G. C.; Borgati, T. F.; Arantes, L. M.; Paula, R. C. d.; Soares, L. F.; do Nascimento, M. F.; Ferreira, M. r. R.; Taranto, A. G.; et al. Synthesis, in vitro antimalarial activity and in silico studies of hybrid kauranoid 1, 2, 3-triazoles derived from naturally occurring diterpenes. *J. Braz. Chem. Soc.* **2016**, *27* (3), 551−565.
(42) Gasteiger, J.; Marsili, M. Iterative partial equalization of orbital electronegativity—a rapid access to atomic charges. *Tetrahedron* **1980**, *36* (22), 3219−3228.
(43) Huey, R.; Morris, G. *AutoDock tools*; The Scripps Research Institute: La Jolla, CA, 2003.

DOI: 10.1021/acsabm.9b00639
ACS Appl. Bio Mater. 2019, 2, 5349−5365

(44) Trott, O.; Olson, A. J. AutoDock Vina: improving the speed and accuracy of docking with a new scoring function, efficient optimization, and multithreading. *J. Comput. Chem.* **2010**, *31* (2), 455−461.
(45) D. E. Shaw Research. *Desmond Molecular Dynamics System*. 2016.
(46) Bhayye, S. S.; Roy, K.; Saha, A. Molecular dynamics simulation study reveals polar nature of pathogenic mutations responsible for stabilizing active conformation of kinase domain in leucine-rich repeat kinase II. *Struct. Chem.* **2018**, *29* (3), 657−666.
(47) Guvench, O.; MacKerell, A. D. Comparison of protein force fields for molecular dynamics simulations. *Methods Mol. Biol.* **2008**, *443*, 63−88.
(48) Essmann, U.; Perera, L.; Berkowitz, M. L.; Darden, T.; Lee, H.; Pedersen, L. G. A smooth particle mesh Ewald method. *J. Chem. Phys.* **1995**, *103* (19), 8577−8593.
(49) Kräutler, V.; Van Gunsteren, W. F.; Hünenberger, P. H. A fast SHAKE algorithm to solve distance constraint equations for small molecules in molecular dynamics simulations. *J. Comput. Chem.* **2001**, *22* (5), 501−508.
(50) Hünenberger, P. H. Thermostat algorithms for molecular dynamics simulations. *Adv. Polym. Sci.* **2005**, *173*, 105−149.
(51) Nosé, S. A unified formulation of the constant temperature molecular dynamics methods. *J. Chem. Phys.* **1984**, *81* (1), 511−519.
(52) Bauri, K.; Pant, S.; Roy, S. G.; De, P. Dual pH and temperature responsive helical copolymer libraries with pendant chiral leucine moieties. *Polym. Chem.* **2013**, *4* (14), 4052−4060.
(53) Moad, G.; Chong, Y. K.; Postma, A.; Rizzardo, E.; Thang, S. H. Advances in RAFT polymerization: the synthesis of polymers with defined end-groups. *Polymer* **2005**, *46* (19), 8458−8468.
(54) Sarkar, K.; Srivastava, R.; Chatterji, U.; Kundu, P. Evaluation of chitosan and their self-assembled nanoparticles with pDNA for the application in gene therapy. *J. Appl. Polym. Sci.* **2011**, *121* (4), 2239−2249.
(55) Sarkar, K.; Meka, S. R. K.; Madras, G.; Chatterjee, K. A self-assembling polycationic nanocarrier that exhibits exceptional gene transfection efficiency. *RSC Adv.* **2015**, *5* (111), 91619−91632.
(56) Yazdanbakhsh, K.; Lomas-Francis, C.; Reid, M. E. Blood groups and diseases associated with inherited abnormalities of the red blood cell membrane. *Transfusion Medicine Reviews* **2000**, *14* (4), 364−374.
(57) Sunshine, J. C.; Peng, D. Y.; Green, J. J. Uptake and Transfection with Polymeric Nanoparticles Are Dependent on Polymer End-Group Structure, but Largely Independent of Nanoparticle Physical and Chemical Properties. *Mol. Pharmaceutics* **2012**, *9* (11), 3375−3383.
(58) Shi, J.; Choi, J. L.; Chou, B.; Johnson, R. N.; Schellinger, J. G.; Pun, S. H. Effect of Polyplex Morphology on Cellular Uptake, Intracellular Trafficking, and Transgene Expression. *ACS Nano* **2013**, *7* (12), 10612−10620.
(59) Pezzoli, D.; Giupponi, E.; Mantovani, D.; Candiani, G. Size matters for in vitro gene delivery: investigating the relationships among complexation protocol, transfection medium, size and sedimentation. *Sci. Rep.* **2017**, *7*, 44134.
(60) Lunnoo, T.; Assawakhajornsak, J.; Puangmali, T. In Silico Study of Gold Nanoparticle Uptake into a Mammalian Cell: Interplay of Size, Shape, Surface Charge, and Aggregation. *J. Phys. Chem. C* **2019**, *123* (6), 3801−3810.
(61) Gratton, S. E. A.; Ropp, P. A.; Pohlhaus, P. D.; Luft, J. C.; Madden, V. J.; Napier, M. E.; DeSimone, J. M. The effect of particle design on cellular internalization pathways. *Proc. Natl. Acad. Sci. U. S. A.* **2008**, *105* (33), 11613−11618.

DOI: 10.1021/acsabm.9b00639
ACS Appl. Bio Mater. 2019, 2, 5349−5365